

Assessment of uranium nitride interatomic potentials

Mohamed AbdulHameed^a, Benjamin Beeler^{a,b,*}, Conor O.T. Galvin^c, Michael W.D. Cooper^c

^a*Department of Nuclear Engineering, North Carolina State University, Raleigh, NC 27695*

^b*Idaho National Laboratory, Idaho Falls, ID 83415*

^c*Los Alamos National Laboratory, Los Alamos, NM 87545*

Abstract

Uranium mononitride (UN) is a promising nuclear fuel due to its high fissile density, high thermal conductivity, and suitability for reprocessing. In this study, two uranium nitride interatomic potentials are assessed: Tseplyaev and Starikov's angular-dependent potential and Kocevski *et al.*'s embedded atom model potential. Predictions of the thermophysical and elastic properties of UN, UN₂, and α - and β -U₂N₃ computed using both potentials are assessed and compared to available experimental data. The Tseplyaev potential performs better with the energetic aspects of UN, e.g., specific heat capacity and point defect formation energies, whereas the Kocevski potential performs better with the structural aspects of UN, e.g., thermal expansion as well as with the elastic properties. The reasons why the Kocevski potential underestimates the UN specific heat are explained by examining the UN phonon properties modeled using both potentials. The Kocevski potential shows better identification of the mechanical stability ranges of UN, UN₂, and α - and β -U₂N₃, reasonably predicting the melting point of UN and predicting stable structures for UN₂ and α - and β -U₂N₃. On the other hand, the Tseplyaev potential predicts a premature phase change of both UN and UN₂ and cannot stabilize α - nor β -U₂N₃. However, the Kocevski potential cannot predict a stable α -U phase and is thus not suitable for the calculation of formation energies for non-stoichiometric point defects.

Keywords: uranium nitride, thermophysical properties, molecular dynamics, phonons, point defects

1. Introduction

Since the 2011 Fukushima Daiichi accident in Japan, research efforts have been directed to develop advanced nuclear fuels that have improved performance in extreme conditions compared to UO₂ while maintaining thermodynamic and mechanical stability [1]. One such fuel candidate is uranium mononitride (UN), which has shown many positive characteristics including high fissile density, high thermal conductivity, good dissolution in nitric acid making it compatible with the PUREX process, good chemical compatibility with most potential cladding materials, and longer fuel residence time [2, 3, 4]. However, it has also

*Corresponding author

Email address: bwbeeler@ncsu.edu (Benjamin Beeler)

9 suffered some drawbacks that historically hindered its industrial adoption, including com-
10 plicated fabrication processes, high fuel cost owing to the need for N-15 enrichment, low
11 resistance to oxidation by high-temperature steam, and high swelling rates [2, 3, 4].

12 UN has not been investigated as widely as oxide fuels, and many aspects of its behavior
13 at high temperatures and under irradiation are not well understood [5]. To address its
14 drawbacks and build a case for its practical use in light-water and advanced reactors, UN
15 properties should be well-understood at the atomic and mesoscales. Multiscale multiphysics
16 fuel performance models can provide a pathway for the descriptive and predictive evolution
17 of nuclear fuels and are especially valuable in cases where experimental data is limited. These
18 models, however, require many input parameters from lower-length scale simulation methods
19 like density functional theory (DFT) and molecular dynamics (MD).

20 Many DFT studies have been conducted on UN to predict its electronic structure and
21 magnetic ordering [6, 7, 8, 9, 10] as well as to understand the properties of its point de-
22 fects [11, 12, 13, 14], impurities [15], and fission products [16, 17, 18, 19]. However, DFT is
23 computationally demanding and has limitations in system size and simulation time. MD sim-
24 ulations can overcome these limitations and offer more flexibility in predicting fuel behavior
25 at finite temperatures. Still, the accuracy of MD results is highly dependent on the quality
26 of the interatomic potentials employed. Therefore, a reliable UN interatomic potential is a
27 necessity.

28 For UN, several interatomic potentials exist in the literature. Kurosaki *et al.* [20, 21] de-
29 veloped a Busing-Ida type potential which they used to predict thermal expansion, constant-
30 pressure specific heat capacity, and thermal conductivity. Calculated properties qualitatively
31 agree with experimental results at low temperatures and exhibit an increasing underestima-
32 tion with increasing temperature. Kurosaki *et al.* mention the values of potential parameters
33 without units, which makes it hard to further assess its behavior. Chen *et al.* [22] used the
34 Chen–Möbius lattice inversion method to derive three Morse-type pair potentials for the
35 U-U, N-N, and U-N interactions. The potential was then used to predict thermal expansion
36 and compressibility with a moderate qualitative agreement. However, Morse-type potentials
37 cannot capture the nature of atomic bonding, especially in covalent solids such as UN [23].

38 Kuksin *et al.* [24] developed an angular-dependent potential (ADP) fitted to DFT calcu-
39 lations. The potential was modified in a later paper by Tseplyaev and Starikov [25], and used
40 to calculate point defect formation and migration energies and to predict the UN pressure-
41 induced $Fm\bar{3}m \rightarrow R\bar{3}m$ phase transition. However, the authors didn't consider the effect of
42 stoichiometry on defect formation energies, and their methodology to calculate the U and
43 N chemical potentials is not reported. They also show evidence of the potential's capability
44 to predict some basic properties of UN_2 and U_2N_3 . Li and Murphy [26] have later used this
45 potential to study self-diffusion in hypo-stoichiometric UN.

46 Kocevski *et al.* [27] developed an embedded-atom method (EAM) potential fitted to
47 experimental thermal expansion and single crystal elastic constants, as well as formation
48 energies of stoichiometric point defects from DFT calculations. The potential [..¹] was used
49 to calculate the elastic properties and temperature-dependent heat capacity[..²]. However,

¹removed: reproduced observed

²removed: with reasonable agreement and was also

50 the authors assumed UN to be an isotropic material, which is not true as will be explained in 3.3,
51 and the heat capacity was underestimated at high temperatures. Also, the potential was used to
52 study Xe diffusion in UN.

53 Tseplyaev and Starikov's ADP (hereafter referred to as the Tseplyaev potential) and Ko-
54 cevski *et al.*'s EAM potential (hereafter referred to as the Kocevski potential) are promising
55 candidate potentials by their construction that attempts to model the complex bonding en-
56 vironment of UN. The main goal of this work is to assess the performance of both potentials
57 and to identify their relevant artifacts and weaknesses by performing MD simulations that
58 calculate UN elastic properties, specific heat capacity, and phonon properties. We also cal-
59 culate point defect formation energies using a methodology that removes the arbitrariness in
60 chemical potential determination. Thermophysical and elastic properties of UN_2 and U_2N_3
61 phases are also computed, and their predicted stability is discussed.

62 2. Computational details

63 All MD calculations performed in this work utilize the Large-scale Atomic/Molecular
64 Massively Parallel Simulator (LAMMPS) software package [28] with a time step of 1 fs
65 and periodic boundary conditions applied in all directions. The Phonopy code [29] is used
66 to calculate phonon properties. To obtain the forces calculated by LAMMPS in a format
67 readable by Phonopy, PhonoLAMMPS, an auxiliary tool of the DynaPhoPy code [30], is
68 used. Detailed computational methodologies of all properties are presented in the respective
69 sections.

70 2.1. Structural properties

71 The U-N solid system has three distinct compounds: UN, uranium dinitride (UN_2), and
72 uranium sesquinitride (U_2N_3) [31]. UN has a NaCl crystal structure with a lattice parameter
73 $a = 4.89 \text{ \AA}$ at room temperature [32] and a melting temperature $T_m = 3035 \text{ K}$ at a nitrogen
74 vapor pressure of 1 atm [33]. UN_2 has a fluorite crystal structure with an experimental
75 lattice parameter $a = 5.21 \text{ \AA}$ [34]. U_2N_3 has a bixbyite crystal structure at low temperatures
76 ($\alpha\text{-U}_2\text{N}_3$) and a hexagonal crystal structure at high temperatures ($\beta\text{-U}_2\text{N}_3$) [4]. $\alpha\text{-U}_2\text{N}_3$ has
77 a space group: $Ia\bar{3}$, and a lattice parameter of 10.7 \AA , whereas $\beta\text{-U}_2\text{N}_3$ has a space group:
78 $P\bar{3}m1$, Pearson symbol: $hP5$, and lattice parameters: $a = 3.69 \text{ \AA}$, $c = 5.83 \text{ \AA}$, $z_U = 0.2467$,
79 and $z_N = 0.6470$ [35, 36]. UN_x has the fluorite crystal structure in the composition range
80 of $1.75 \leq x \leq 2.00$, whereas the $\text{UN}_2/\alpha\text{-U}_2\text{N}_3$ solid solution is stable for $1.54 \leq x \leq 1.75$
81 [31]. Additionally, the conventional unit cell of $\alpha\text{-U}_2\text{N}_3$ can be regarded as a $2 \times 2 \times 2$
82 UN_2 supercell with a quarter of the N atoms removed [37]. For these reasons, the names
83 UN_2 and U_2N_3 are often used interchangeably to refer to the $\text{UN}_2/\alpha\text{-U}_2\text{N}_3$ solid solution at
84 low and intermediate temperatures [31, 4]. The $\text{UN}_2/\alpha\text{-U}_2\text{N}_3$ solid solution decomposes at a
85 temperature of either 1324 K [4] or 1405 K [38], the uncertainty being due to the dependence
86 of the U-N phase diagram on the nitrogen vapor pressure [4]. Due to the same uncertainty,
87 $\beta\text{-U}_2\text{N}_3$ exists as a single phase in either the temperature range 1324-1648 K [4] or the range
88 1214-1625 K [38].

89 We compare the UN lattice constant predicted by both potentials through 0 K energy
90 minimization to the experimental value. The UN linear thermal expansion coefficient (LTEC)

⁹¹ predicted by both potentials is also computed. To allow comparison with the Hayes *et al.*
⁹² [32] empirical correlation, the mean LTEC is defined as (assuming isotropic expansion):

$$\alpha_L = \frac{a - a_0}{a_0 (T - T_0)} \quad (1)$$

⁹³ where a is the lattice parameter and a_0 is the lattice parameter at a reference temperature
⁹⁴ $T_0 = 300$ K. It should be noted that this definition of the LTEC is different from the
⁹⁵ thermodynamic definition: $\alpha_L = (1/a)\partial a/\partial T$. To calculate the temperature variation of the
⁹⁶ lattice parameters and LTECs of UN, UN₂, α - and β -U₂N₃, 15 × 15 × 15 supercells of UN,
⁹⁷ UN₂, and α -U₂N₃ (and 8 × 8 × 8 supercells of β -U₂N₃) are equilibrated in the *NPT* ensemble
⁹⁸ for 100 ps and their lattice parameters are averaged over the last 50 ps. Unless otherwise
⁹⁹ stated, these supercell sizes are used in all subsequent calculations.

¹⁰⁰ 2.2. Melting point

¹⁰¹ The thermodynamic definition of melting is the point at which solid and liquid states
¹⁰² co-exist, and thus have the same free energy [39, 40]. However, the melting point predicted
¹⁰³ by MD based on simple heating corresponds to the point at which the solid lattice mechanically
¹⁰⁴ collapses, and is usually overestimated compared to the true one due to the existence
¹⁰⁵ of a free energy barrier to the formation of a solid-liquid interface in perfect supercells.
¹⁰⁶ This barrier leads to a hysteresis effect associated with the necessity to run the simulation
¹⁰⁷ for a sufficient time at a superheated temperature so that a seed of the liquid phase can
¹⁰⁸ spontaneously nucleate [41, 39]. This free-energy barrier can be eliminated by using the
¹⁰⁹ void-induced melting method [39, 40]. Voids (introduced in the supercell in the form of
¹¹⁰ Schottky defects) form local pockets of a liquid-like structure, which effectively introduces
¹¹¹ solid-liquid interfaces. With increasing the number of voids, the free energy barrier to melting
¹¹² decreases, until, for a sufficient number of voids, the predicted melting point reaches a
¹¹³ plateau for a limited range. If too many voids are introduced, the solid becomes mechanically
¹¹⁴ unstable and collapses without a discontinuous solid-to-liquid phase transition [39]. Melting
¹¹⁵ is a first-order phase transition that is signified by a step-like transition in the volume versus
¹¹⁶ temperature curve, or, equivalently, a spike in the specific heat versus temperature curve
¹¹⁷ [42]. Voids within the range 0-2 at. % are introduced into the UN supercells, which are then
¹¹⁸ equilibrated in the *NPT* ensemble for 100 ps, their total energy and volume are averaged
¹¹⁹ over the last 50 ps, and the solid-to-liquid transition temperatures are recorded for each ³
¹²⁰ [vacancy concentration].

¹²¹ 2.3. Elastic properties

¹²² The elastic stiffness tensor, C_{ij} , is computed using the explicit deformation method [43].
¹²³ At 0 K, supercells of UN, UN₂, α - and β -U₂N₃ are relaxed and then strains are applied
¹²⁴ to the $\pm x$ -, $\pm y$ -, and $\pm z$ -directions with magnitudes of 0.005%, 0.01%, and 0.05%. The
¹²⁵ supercell energy is minimized with a constant volume and the stress tensor is calculated.
¹²⁶ For the finite-temperature calculations, averaged UN and UN₂ lattice parameters at each
¹²⁷ temperature are used to construct supercells of the same size, whereas, for α - and β -U₂N₃,

³removed: void fraction

128 the supercells are initially equilibrated in the *NPT* ensemble for 50 ps. Supercells are then
 129 equilibrated for 20 ps using a Langevin thermostat, the Langevin thermostat is then switched
 130 off and strains of 0.5%, 0.1%, and 1.5% are applied to the same directions under the *NVE*
 131 ensemble. Finally, the stress tensor components are then averaged over the next 10 ps. For
 132 the UN, UN_2 , and $\alpha\text{-U}_2\text{N}_3$ crystals with cubic symmetry, only three of the elastic constants
 133 are independent: C_{11} , C_{12} , and C_{44} [44], whereas, for the hexagonal structure of $\beta\text{-U}_2\text{N}_3$, five
 134 elastic constants are independent: C_{11} , C_{12} , C_{13} , C_{33} and C_{44} [45]. Various strains are used
 135 at 0 K and finite temperatures to make sure the elastic properties are strain-independent.
 136 Larger strains are used at finite temperatures to reduce uncertainties arising from thermal
 137 fluctuations.

138 Polycrystalline elastic moduli are computed from the single-crystal elastic constants ac-
 139 cording to the Voigt-Reuss-Hill (VRH) approach [46, 44, 43] as Hill averages of upper Voigt
 140 limits and lower Reuss limits on the bulk and shear moduli. The form of the VRH elas-
 141 tic moduli is included in [Appendix A](#). The elastic stability criteria are also checked for
 142 UN, UN_2 , and α - and $\beta\text{-U}_2\text{N}_3$. For cubic crystals, the conditions for elastic stability are
 143 $C_{11} - C_{12} > 0$, $C_{11} + 2C_{12} > 0$, and $C_{44} > 0$, whereas, for hexagonal crystals, the elastic
 144 stability conditions are: $C_{11} > |C_{12}|$, $2C_{13}^2 < C_{33}(C_{11} + C_{12})$, and $C_{44} > 0$ [47]. [The stability](#)
 145 [of the solid crystal structure is also judged by observing the radial distribution functions \(RDFs\)](#)
 146 [calculated by OVITO. For a specific crystal structure, the RDF is characterized by distinct peaks.](#)
 147 [A phase transformation to a different crystal structure is characterized by the change of peak](#)
 148 [positions, whereas for a liquid, the RDF is characterized by a single peak after which the RDF](#)
 149 [assumes a value of about 1](#) [48].

150 The Anderson method is one of the standard methods to calculate the Debye temperature
 151 from the 0 K elastic constants according to the equations [46]:

$$\theta_D = \frac{\hbar}{k_B} \left(\frac{3q}{4\pi} \frac{N_A \rho}{M} \right)^{1/3} v_0 \quad (2)$$

$$v_0 = \left[\frac{1}{3} \left(\frac{2}{v_t^3} + \frac{1}{v_l^3} \right) \right]^{-1/3} \quad (3)$$

$$v_t = \sqrt{\frac{G}{\rho}} \quad (4)$$

$$v_l = \sqrt{\frac{3B + 4G}{3\rho}} \quad (5)$$

152 where q is the number of atoms per formula unit ($q = 2$ for UN), M is the molecular weight,
 153 v_0 is the average sound velocity, v_t is the average transverse sound velocity for an isotropic
 154 material, and v_l is the average longitudinal sound velocity for an isotropic material. Another
 155 method to calculate the Debye temperature for cubic crystals is the semi-empirical Siethoff-
 156 Ahlborn method based on the room-temperature elastic constants [49]:

$$\theta_D = C \left(\frac{aqG'}{M} \right)^{1/2} \quad (6)$$

160

$$G' = \left[C_{44} \left(\frac{(C_{11} - C_{12})C_{44}}{2} \right)^{1/2} \left(\frac{C_{11} - C_{12} + C_{44}}{3} \right) \right]^{1/3} \quad (7)$$

161 where a is the lattice constant, and C is an empirical parameter that depends on the crystal
 162 structure ($C = 18.56$ K for the NaCl structure). q and M have the same meaning as in the
 163 Anderson method. Both methods are utilized for the determination of θ_D in this work.

164 *2.4. Specific heat capacity*

165 Because UN behaves as a metallic solid [19, 50], its constant-pressure specific heat ca-
 166 pacity, C_P , has two main contributions: lattice, C_{lat} , and electronic, C_{elec} , specific heat
 167 capacities, where electron-phonon interactions have been neglected. To calculate C_{lat} , su-
 168 percells are equilibrated in the NPT ensemble for 100 ps and their total energy is averaged
 169 over the last 50 ps. All specific heats are computed as the slope of the potential energy as a
 170 function of temperature using three-point centered finite differences with 50 K increments.
 171 C_{lat} can be decomposed into the following contributions [51, 52]:

$$C_{\text{lat}} = C_V + C_{\text{exp}} + C_{\text{anharm}} + C_d \quad (8)$$

172 where C_V is the constant-volume specific heat, C_{exp} is the contribution due to thermal
 173 expansion, C_{anharm} is the anharmonic non-expansive contribution, and C_d is the contribution
 174 due to defect generation. C_V is calculated by restricting the supercells to the equilibrium 0
 175 K volume and averaging the total energy within the NVT ensemble. C_{exp} can be calculated
 176 from [53]:

$$C_{\text{exp}} = 9\alpha_L^2 BV_m T \quad (9)$$

177 where α_L is the linear thermal expansion coefficient, B is the bulk modulus, and V_m is the
 178 molar volume. Neglecting C_d for perfect crystals, C_{anharm} (Fig. 4d) is calculated from:

$$C_{\text{anharm}} = C_{\text{lat}} - C_V - C_{\text{exp}} \quad (10)$$

179 C_{elec} is estimated from [54, 20, 50]:

$$C_{\text{elec}} = \frac{\pi}{3} g(\epsilon_F) N_A k_B^2 T = \gamma T \quad (11)$$

180 where $g(\epsilon_F)$ is the density of states (DOS) at the Fermi level (states/eV-atom), and γ is the
 181 electronic specific heat coefficient (J/mol-K²). Samsel-Czekala *et al.* [6] reported a value of γ
 182 = 3.7 mJ/mol-K² based on their electronic-structure calculation, and this is the value used in
 183 our calculations. Kocevski *et al.* [50] reported $g(\epsilon_F) = 2-2.2$ states/eV-atom in their *ab initio*
 184 MD calculation, which gives a value of γ equal to about 1.5-1.7 mJ/mol-K². These γ values
 185 are in large contrast with the experimentally reported values of about 34 mJ/mol-K² [55]
 186 and 50 mJ/mol-K² [56] obtained by fitting heat capacity data. Szpunar *et al.* [57] have also
 187 calculated γ using the Quantum ESPRESSO code and found $\gamma = 17.6$ mJ/mol-K² for the
 188 PBEsol functional and $\gamma = 0.6$ mJ/mol-K² for the non-local hybrid B3LYP functional—both
 189 values being smaller than the experimental ones.

190 *2.5. Phonon properties*

191 To get a deeper understanding of the calculated thermal properties of UN, we study how
 192 the Tseplyaev and Kocevski potentials model the UN phonon properties. Harmonic force
 193 constants are calculated using the finite displacement method [58]. To compute accurate
 194 forces using small displacements, initial UN structures must be fully relaxed [59], which was
 195 accomplished using static energy minimization in LAMMPS. The equilibrium UN lattice
 196 constants of each potential are then used to construct $3 \times 3 \times 3$ UN primitive cells (54
 197 atoms). PhonoLAMMPS, coupled to LAMMPS, is used to apply a displacement of 0.01 Å
 198 to the supercell and get the interatomic forces of the displaced configurations, where the
 199 required displacement patterns are determined by the symmetry of the supercell. Phonopy
 200 reads the generated forces and calculates symmetrized harmonic force constants from [60, 61]:

$$K_{ls\alpha,l's'\beta} = -\frac{\partial F_{ls\alpha}}{\partial u_{l's'\beta}} \quad (12)$$

201 where $K_{ls\alpha,l's'\beta}$ is a second-order (harmonic) force constant, l labels the unit cells, s labels the
 202 atoms within each unit cell, α and β label Cartesian coordinates, $u_{l's'\beta}$ is the displacement of
 203 atom s' within unit cell l' in the β direction and the force $F_{ls\alpha} = -\partial U / \partial u_{ls\alpha}$ where U is the
 204 lattice potential energy. The phonon band structure is calculated along the high symmetry
 205 k -path: $\Gamma-X-K-\Gamma-L$ to allow comparison with experimental results. To compute the phonon
 206 DOS, the reciprocal space is sampled by a Γ -centered $100 \times 100 \times 100$ mesh, and the linear
 207 tetrahedron method is used for integration in the Brillouin zone.

208 *2.6. Point defect formation energies*

209 The formation energy of uncharged point defects at $T = 0$ K is defined as [62, 63, 64]:

$$E_f = E_d - E_p - \sum_i n_i \mu_i = \delta E - \sum_i n_i \mu_i \quad (13)$$

210 where E_d and E_p are the energies of the defective and perfect supercells, respectively, n_i is
 211 the number of atoms of type i removed ($n_i < 0$) or added ($n_i > 0$) to form the defect, and
 212 μ_i is the chemical potential of the i th species. δE is termed the “raw” formation energy [62].
 213 For Schottky defects (SD) and Frenkel defects (FD), the crystal’s stoichiometry does not
 214 change, and special cases of Eq. (13) exist. For Frenkel defects, the formation energy is just
 215 $E_f = E_d - E_p$, whereas, for a Schottky defect, the formation energy is:

$$E_f = E_d - \frac{N - A}{N} E_p \quad (14)$$

216 where N is the total number of atoms in the supercell, and A is the number of atoms per
 217 formula unit ($A = 2$ for UN) [65].

218 Chemical potentials represent the energy of the reservoirs with which atoms are being
 219 exchanged [63, 66], and the proper choice of the chemical potentials in Eq. (13) depends on
 220 phase stabilities of the considered system [66]. For a binary compound AB, the chemical
 221 potentials of A and B vary from A-rich to B-rich compositions displaying a discontinuity at
 222 the stoichiometric composition [67, 62, 68]. While numerous formalisms exist in the literature
 223 for determining the chemical potentials of relevant species [62, 13, 67, 68, 63, 27], the method

of Huang *et al.* [69, 19] is used in this work. In this method, upper and lower bounds are imposed on the chemical potential to capture its dependence on stoichiometry; these bounds are dictated by the cohesive energies of the competing phases at very low temperatures. Based on an examination of the UN phase diagram [38, 4], it can be argued that the bounds on the U and N chemical potentials at very low temperatures are governed by transformations to α -U for U-rich conditions (i.e., co-existence of UN and α -U), and transformation to UN₂ for N-rich conditions (i.e., co-existence of UN and UN₂) [69, 19]. Accordingly, the U and N chemical potentials are calculated from [19]:

$$E_c(U_xN_y) = x\mu_U + y\mu_N \quad (15)$$

where $E_c(U_xN_y)$ is the cohesive energy (energy per formula unit). Eq. (15) is solved for UN and α -U to get the U-rich chemical potentials, and for UN and UN₂ to get the N-rich chemical potentials [69, 19]. The chemical potentials at stoichiometric conditions are the averages of these two bounds [68].

Although many DFT studies have investigated point defect formation energies in UN [11, 13, 14, 24, 25, 27], only Yang and Kaltsoyannis [19] and Kocevski *et al.* [10] have looked at their variation with stoichiometry. Yang and Kaltsoyannis used the PW91 functional, whereas Kocevski *et al.* used the PBE and AM05 functionals, with and without an added on-site Coulomb repulsion term (+U), and found a variation of the defect formation energies with different DFT methodologies.

3. Results

3.1. Structural properties

The UN lattice parameters predicted by the Tseplyaev and Kocevski potentials at 0 K are 4.81 Å and 4.90 Å, respectively, compared to the experimental room temperature (RT) value of 4.89 Å [32]. As can be seen in Fig. 1a, the Kocevski potential is closer in comparison to the [...] experimental results of both Hayes *et al.* [32] and Liu *et al.* [70], whereas the Tseplyaev potential slightly underestimates it. The linear thermal expansion coefficient (LTEC) is shown in Fig. 1b. The Tseplyaev potential predicts a temperature-independent thermal expansion up to about 1000 K and then predicts a fifth-order power-law expansion—a trend that does not agree with experimental observations. On the other hand, while the Kocevski potential underestimates the UN LTEC with a larger error than that of the Tseplyaev potential, [...] it predicts a trend very similar to that given by Hayes *et al.* and Liu *et al.* This is in accordance with the recently published results from Galvin *et al.* [71].

3.2. Melting point

The melting temperature predicted by both potentials is shown in Fig. 2. According to Alavi and Thompson [39], the thermodynamic melting point is determined as the value of the range over which the melting temperature appears to be independent of the [...] vacancy

⁴removed: empirical correlation of the UN lattice parameter

⁵removed: but predicts nearly the same trend as a function of temperature observed in experiments.

⁹removed: void fraction

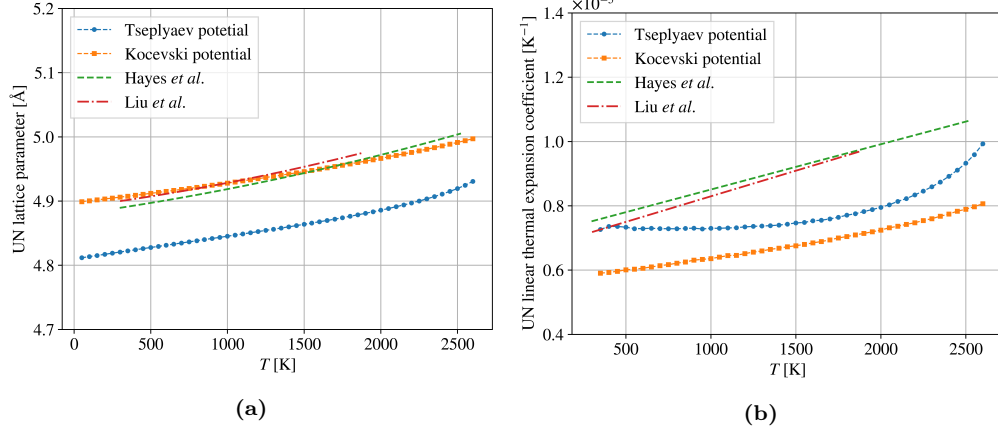


Figure 1: (a) UN lattice parameter calculated by both potentials and compared to the [\[..⁶\]](#)experimental data of Hayes *et al.* [\[..⁷\]](#)[\[32\]](#) and Liu *et al.* [\[70\]](#). (b) UN linear thermal expansion coefficient calculated by both potentials and compared to the experimental data of Hayes *et al.* [\[..⁸\]](#)[\[32\]](#) and Liu *et al.* [\[70\]](#).

259 concentration. Based on this measure, the Tseplyaev potential predicts thermodynamic melting
 260 at about 2700 K, whereas the Kocevski potential predicts it at about 3100 K; a value
 261 that is close to the experimental value of 3035 K estimated from the Hayes *et al.* correlation
 262 at a nitrogen vapor pressure of 1 atm [\[33\]](#). It can be concluded that the Kocevski potential
 263 gives a better prediction of the phase stability range of UN because its predicted melting
 264 point is closer to the experimental data, whereas the Tseplyaev potential predicts a slightly
 265 premature melting of UN.

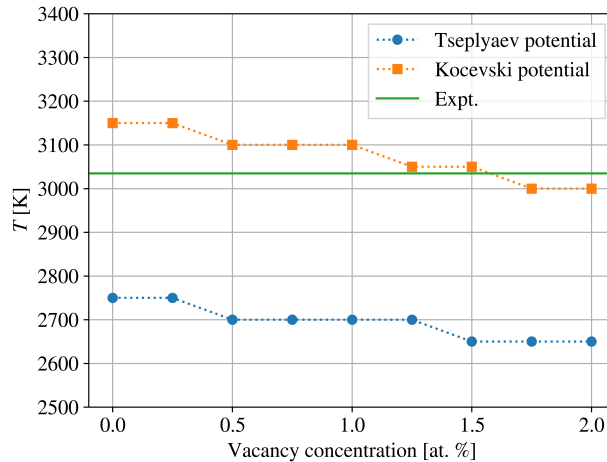


Figure 2: UN melting point as predicted by both potentials as a function of [\[..¹⁰\]](#)vacancy concentration using the void-induced melting method. The experimental melting temperature (3035 K) is taken from the Hayes *et al.* correlation at a nitrogen vapor pressure of 1 atm [\[33\]](#).

266 3.3. Elastic properties

267 The UN elastic constants calculated at 0 K using both potentials are shown in [Table 1](#).
 268 A much larger error is associated with the values of C_{11} and C_{44} calculated by the Tseplyaev

potential compared to those calculated by the Kocevski potential, whereas the Tseplyaev potential estimation of C_{12} is slightly better. It was found that UN elastic constants calculated at 0 K using the Tseplyaev potential show a discontinuity compared to finite-temperature values, which contradicts the third law of thermodynamics that requires a near-zero slope of the elastic constants versus T curves as T approaches 0 K [72]. This discontinuity can be attributed to static energy minimization predicting metastable states of strained UN supercells. Thermal motion is likely to lead the strained supercells to a global minimum of the potential energy hypersurface. For this reason, we also compute the elastic constants at 1 K. The elastic constants, moduli, and Poisson's ratio at finite temperatures are shown in Fig. 3. When calculated by the Kocevski potential, 1 K elastic constants show no significant difference from those calculated at 0 K, whereas 1 K elastic constants calculated by the Tseplyaev potential led to the disappearance of the discontinuity. All computed elastic constants were found to be independent of the amount of strain within the computational uncertainty.

Table 1: UN elastic constants (GPa) as calculated by both potentials. Experimental elastic constants are at 290 K.

	C_{11}	C_{12}	C_{44}	B
Tseplyaev potential (0 K)	586.6	110.5	54.7	269.2
Tseplyaev potential (1 K)	602.1	125.5	54.9	284.4
Kocevski potential (0 K)	425.4	117.0	71.0	219.8
Expt. [73]	423.9	98.1	75.7	206.7

In Fig. 3a, C_{12} and C_{44} computed by the Tseplyaev potential show a good agreement with experimental values at RT, whereas it overestimates RT C_{11} by more than 35%. On the other hand, all elastic constants calculated by the Kocevski potential agree well with the experimental values at RT. Regarding the elastic moduli (Fig. 3b), the Tseplyaev potential reproduces the experimental Young's modulus by Hayes *et al.* [74] at RT, while the RT value calculated by the Kocevski potential can be regarded as an average estimate of the value of Hayes *et al.* [74] and Frazer *et al.* [76]. The Tseplyaev potential overestimates the UN bulk modulus by more than 40%, whereas the Kocevski potential shows a better prediction and only overestimates it by about 15%. Both potentials slightly underestimate the shear modulus, G . The Kocevski potential shows a good prediction of the UN Poisson's ratio compared to the experimental value at RT with an error of about 10% (Fig. 3c) and predicts a [..]¹¹ more or less constant Poisson's ratio as assumed by Hayes *et al.* [74]. However, the Tseplyaev potential overestimates the RT Poisson's ratio by about 20% and predicts a decrease of the Poisson's ratio with increasing temperature, which is related to the significant softening of the bulk modulus.

The only experimental measurements of the temperature variation of the UN elastic properties are the studies by Padel and de Novion [75] and by Frazer *et al.* [76] on the temperature dependence of UN Young's modulus. Padel and de Novion [75] report a temperature dependence of Young's modulus of the form:

$$E(T) = E_0 (1 - 2.375 \times 10^{-5} T) \quad (16)$$

¹¹removed: slight increase with increasing temperature, which is the expected trend

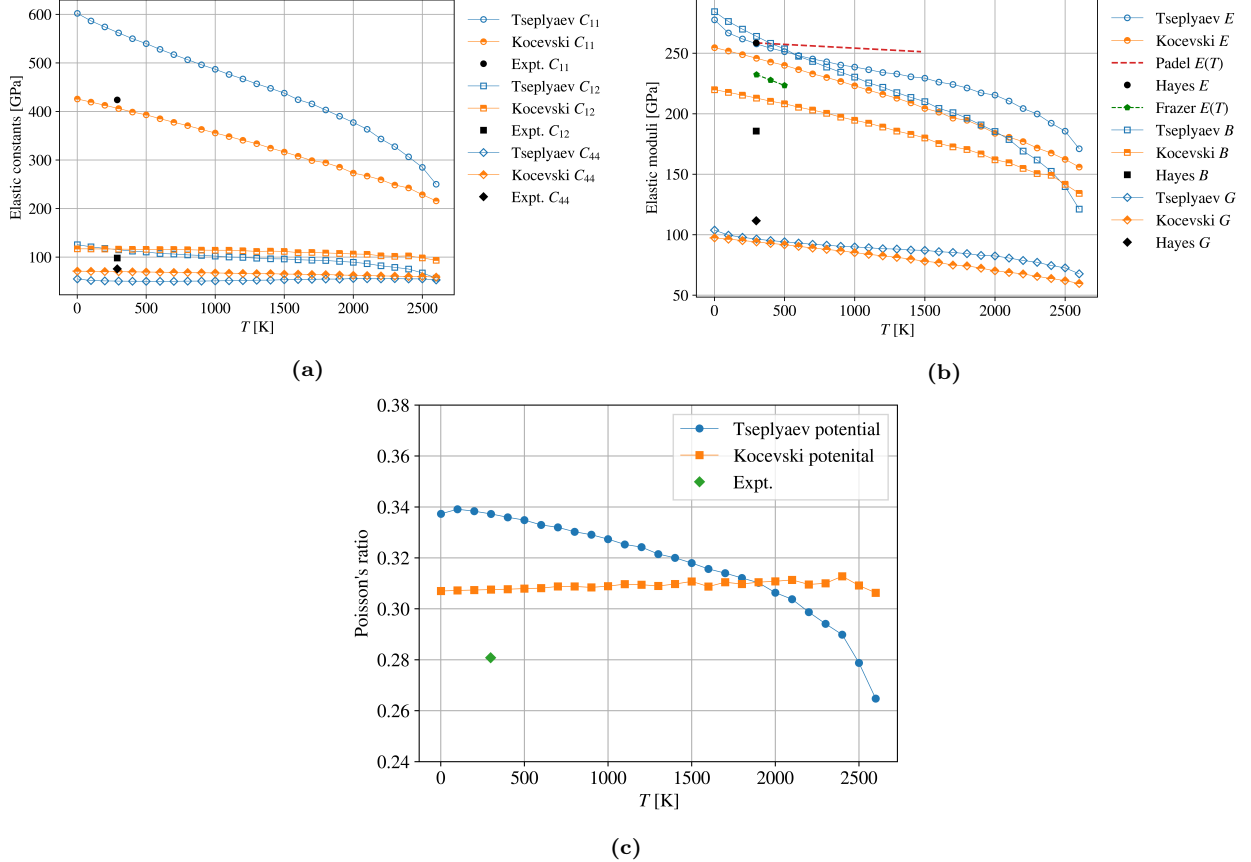


Figure 3: Computations of the temperature variation of (a) UN elastic constants, C_{11} , C_{12} , and C_{44} , (b) UN Young's modulus, E , bulk modulus, B , and shear modulus, G , and (c) Poisson's ratio as calculated by both potentials. The experimental data points in (a) are from Salleh *et al.* (1986) [73]. The experimental data points in (b) and (c) are from Hayes *et al.* (1990) [74]. The experimental variation of Young's modulus with temperature in (b) is due to Padel and de Novion [75], which Hayes *et al.* assumed to be valid also for UN's bulk and shear moduli, and due to the more recent study by Frazer *et al.* [76].

301 in the temperature range of 298-1473 K, [..¹²] whereas Frazer *et al.* predict a dependence of
302 the form:

$$E(T) = 245.78 - 0.0449T \quad (17)$$

303 in the temperature range of 300-500 K.

304 Eq. (16) predicts a softening rate that is much slower than that predicted by either
305 potential as is obvious in Fig. 3b, whereas, despite its limited range, the softening rate implied
306 by Frazer *et al.*'s data [76] seems to agree better with that predicted by both potentials. Hayes
307 *et al.* [74] assumed the temperature dependence of Eq. (16) applies for all elastic properties
308 except for Poisson's ratio, which they assumed to be independent of temperature. This
309 latter assumption agrees with Poisson's ratio calculated by the Kocevski potential which
310 can be approximated as temperature-independent. Kocevski *et al.* [27] also calculated the
311 temperature variation of the UN elastic properties using their potential. Our results generally

¹²removed: with no experimental data to support it,

312 agree with theirs for all elastic properties except for Poisson's ratio which they estimated
 313 to be ~ 0.22 at RT compared to the experimental value of ~ 0.28 and our value of 0.31.
 314 The reason for this discrepancy is that they calculated Poisson's ratio from the formula:
 315 $\nu = C_{12}/(C_{11} + C_{12})$, which assumes the elastic constants are of an isotropic material which
 316 is not the case for UN, as $C_{11} - C_{12} \neq 2C_{44}$ [73, 77].

317 The computed Debye temperatures using different methods are given in [Table 2](#) and
 318 compared to values reported in the literature. Values calculated in this work fall within the
 319 range 355-368 K and agree with the values [[..¹³](#)] measured by Adachi *et al.* [78], Scarbrough
 320 *et al.* [56], and Whaley *et al.* [79]. A large scatter is evident in the experimental Debye
 321 temperature values which range from 181-364 K. Scarbrough *et al.* [56] suspected that the
 322 values reported by Counsell *et al.* [55] and Westrum and Barber [80] (276 K and 289 K,
 323 respectively) are likely affected by the presence of magnetic specific heat. Salleh *et al.* [73]
 324 report a value of $\theta_D = 282$ K without any reference to the method they used to derive it.
 325 It's interesting to note that when Salleh *et al.*'s RT elastic constants are substituted into the
 326 Anderson and Siethoff-Ahlborn methods, they give values of $\theta_D = 365$ K and $\theta_D = 373$ K,
 327 respectively.

Table 2: UN Debye temperature values estimated in this work and reported in the literature.

Method	Reference	θ_D
Tseplyaev potential + Anderson method	This work	365 K
Tseplyaev potential + Siethoff-Ahlborn method	This work	356 K
Kocevski potential + Anderson method	This work	355 K
Kocevski potential + Siethoff-Ahlborn method	This work	356 K
Sound-velocity measurements in polycrystalline UN	Adachi <i>et al.</i> [78]	339 K
Sound-velocity measurements in polycrystalline UN	Whaley <i>et al.</i> [79]	361-364 K
Specific heat measurements in the temperature range 1.3-4.6 K	Scarbrough <i>et al.</i> [56]	324 K
Specific heat measurements in the temperature range 5-350 K	Westrum and Barber [80]	289 K
Specific heat measurements in the temperature range 11-320 K	Counsell <i>et al.</i> [55]	276 K
Not reported	Salleh <i>et al.</i> [73]	282 K
Derived from the UN phonon spectrum measured at 4.2 K	Baranov <i>et al.</i> [81]	181 K
DFT calculation	Mei <i>et al.</i> [9]	244 K

328 Baranov *et al.* [81] made a mistake in their estimation of the Debye temperature. They
 329 computed the Debye frequency using $\omega_D = v_0 k_D$, where v_0 is the average phonon group
 330 velocity estimated from [Eq. \(3\)](#) with $v_0 = 2990$ m/s (given that $v_l = 4740$ m/s and $v_t =$
 331 2691 m/s) and $k_D = (6\pi^2/\Omega)^{1/3}$, where Ω , the volume of the primitive UN unit cell, is equal
 332 to $a^3/4$, a being the lattice parameter [82]. Instead of using the volume of the *primitive* UN
 333 unit cell, they used the volume of the conventional unit cell, which led to an underestimation
 334 of the Debye temperature $\theta_D = \hbar\omega_D/k_B$. Instead of $\theta_D = 181$ K, their appropriate value
 335 should have been $\theta_D = 289$ K. Interestingly, when using the formula $v_0 = (v_l + 2v_t)/3$ to
 336 average the velocities of the acoustic branches [82], $v_0 = 3373$ m/s and Baranov *et al.*'s
 337 $\theta_D = 326$ K, which is close to our calculated values. Based on this analysis, it can be
 338 concluded that the variation of the experimental Debye temperature between the two ranges
 339 276-289 K and 324-365 K can partly be attributed to the differences in the averaging formulas

¹³removed: calculated by

340 used to estimate the average acoustic phonon group velocity. Another contribution is the
341 antiferromagnetic nature of UN which leads the θ_D estimated from specific heat data to
342 be smaller than that estimated from elastic constants as pointed out by Whaley *et al.* [79].
343 Based on this analysis, we can conclude that the average UN θ_D is around 362 K as estimated
344 from both experimental and computed elastic constants.

345 *3.4. Specific heat capacity*

346 UN C_P and its components are shown in Fig. 4. C_{exp} (Fig. 4c) is calculated from functions
347 fitted to the UN LTEC (Eqs. (B.1) and (B.2)) and bulk modulus (Eqs. (B.3) and (B.4)), and
348 C_{anharm} (Fig. 4d) is calculated from functions fitted to the values of C_P (Eqs. (B.5) and (B.6))
349 and C_V (Eqs. (B.7) and (B.8)) calculated by both potentials. It can be seen in Fig. 4a that
350 the Tseplyaev potential compares well with the UN C_P experimental correlation from Hayes
351 *et al.* [33]. However, care must be taken when comparing to the high-temperature values of
352 this correlation as discussed by Galvin *et al.* [71]. Both potentials agree in the computed C_P
353 and C_V up to about 1200 K and 700 K, respectively, whereas at higher temperatures, the
354 Kocevski potential significantly underestimates both C_P and C_V . The Tseplyaev potential
355 predicts that the anharmonic contribution is nearly zero at low and intermediate tempera-
356 tures, and only becomes significant at $T > 1800$ K, whereas the Kocevski potential predicts
357 a minor contribution across the entire temperature spectrum. As can be seen in Fig. 4,
358 the discrepancy between the C_P computed by both potentials (~ 30 J/mol-K at 2500 K)
359 can almost completely be attributed to a difference in the computed C_V (~ 10 J/mol-K at
360 2500 K) and a difference in the estimated C_{anharm} (~ 20 J/mol-K at 2500 K), whereas the
361 difference in the thermal expansion contribution is quite small (~ 1 J/mol-K at 2500 K). It is
362 interesting to note that the structural inaccuracies of the Tseplyaev potential in determining
363 both the bulk modulus and the LTEC nearly balance and cancel out giving a C_{exp} value
364 that is very close to that predicted by the Kocevski potential at low temperatures. That is,
365 the Tseplyaev-potential predictions of UN properties are energetically accurate despite the
366 observed structural and elastic inaccuracies.

367 C_V and C_{anharm} are completely determined by the phonon properties of the material,
368 and, thus, to understand why the Kocevski potential underestimates the UN C_P , a deeper
369 investigation of the UN phonon properties as predicted by both potentials is necessary and
370 will be shown in Section 3.5.

371 *3.5. Phonon properties*

372 The results for the UN phonon properties are shown in Fig. 5. Experimental data for
373 UN phonon band structure and density of states (DOS) were measured by Jackman *et al.*
374 [83] and Aczel *et al.* [84] at temperatures of 4.2 K and 5 K, respectively. Given that
375 anharmonicity should be negligible at these cryogenic temperatures, we have carried out
376 phonon calculations in the harmonic approximation for comparison. It can be observed from
377 the phonon band structure (Fig. 5a) and phonon DOS (Fig. 5b) that both potentials show
378 a good qualitative agreement with the experimentally observed acoustic phonon spectrum
379 while overestimating the acoustic phonon DOS. It can also be seen in Fig. 5a that the
380 Tseplyaev potential only predicts the upper portion of the optical phonon spectrum with

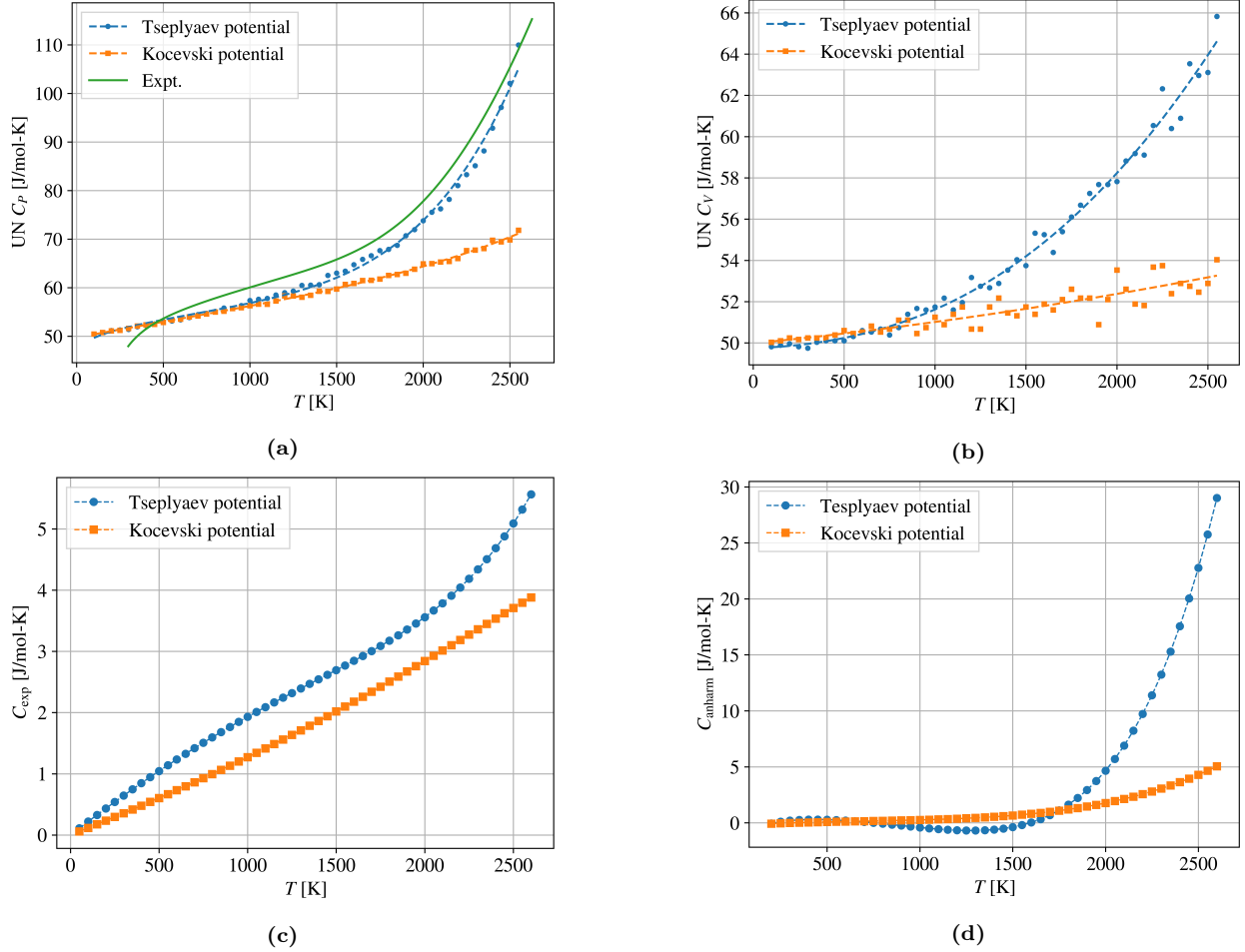


Figure 4: (a) C_P and (b) C_V of UN as calculated by both potentials and compared to the empirical correlation of Hayes *et al.* (1990) [33]. (c) The thermal expansion contribution to the specific heat. (d) The anharmonic non-expansive contribution to the specific heat.

moderate qualitative agreement, whereas it completely misses the lower optical branches. [..]¹⁴ Fig. 5b shows that the optical phonon frequency range predicted by the Kocevski potential is overestimated by about 1.9 THz compared to experimental measurements, incorrectly describing all optical branches.

The acoustic phonon spectrum and low-frequency DOS are related to the vibrations of the heavier uranium atoms, whereas the optical phonon spectrum and high-frequency DOS are related to the vibrations of the lighter nitrogen atoms [81, 45]. Therefore, it can be concluded that both potentials accurately model the uranium atom vibrations whereas only the Tseplyaev potential can qualitatively model the nitrogen atom vibrations. From these results, the Kocevski potential underestimation of the UN C_P compared to that predicted by the Tseplyaev potential can be attributed to the Kocevski potential overestimation of

¹⁴removed: The optical branches predicted by the Tseplyaev potential coincide only for some portion of the k -path because the potential lacks the long-range electrostatic interaction, which is responsible for splitting the longitudinal and transverse optical phonon branches in ionic materials [85].

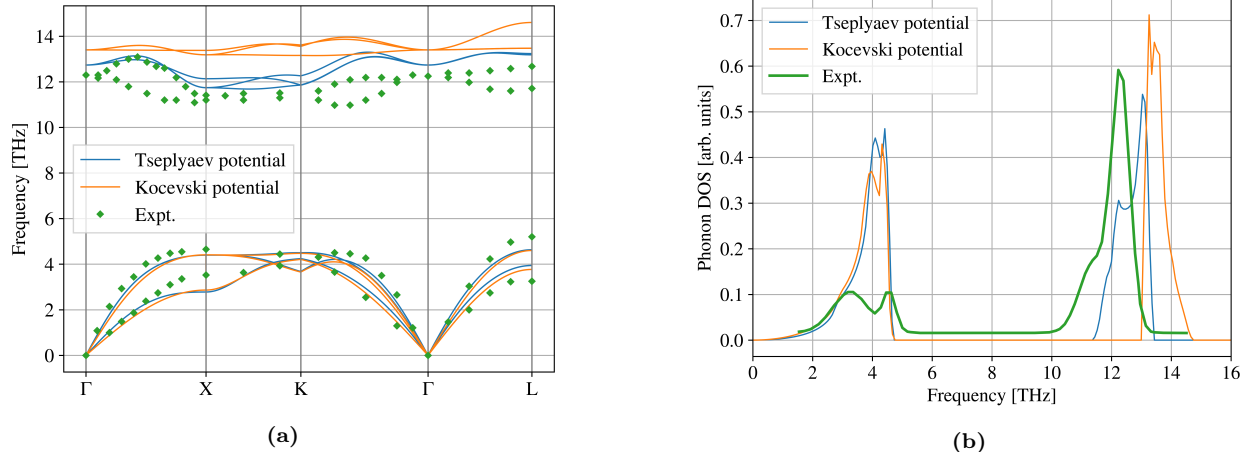


Figure 5: (a) UN phonon band structure as calculated by both potentials and compared to the experimental data of Jackman *et al.* [83]. (b) UN phonon density of states (DOS) as calculated by both potentials and compared to the inelastic neutron scattering data of Aczel *et al.* [84]. The areas under the phonon DOS plots have been normalized to 1 to allow comparison between calculations and the experiment.

392 the optical phonon frequency range. The contribution of the optical phonons to the specific
 393 heat can be treated by the Einstein model. Due to their nearly flat dispersion curve, optical
 394 phonons are approximated within the Einstein model as having a single average frequency,
 395 ω_E , independent of k . From the experimental UN dispersion curve, $\omega_E = 12.0$ THz, whereas
 396 $\omega_E = 12.5$ THz for the Tseplyaev potential, and $\omega_E = 13.9$ THz for the Kocevski potential.
 397 Because phonons are bosons, they follow the Bose-Einstein distribution [45]:

$$f_{BE} = \frac{1}{\exp(\hbar\omega/k_B T) - 1} \quad (18)$$

398 where f_{BE} quantifies the mean number of phonons of frequency ω present in thermal equi-
 399 librium at temperature T [86]. With the Kocevski potential overestimating ω_E , it predicts
 400 a smaller average number of excited optical phonons, which leads to a smaller contribution
 401 of the optical phonons to the UN specific heat. Torres *et al.* [59] also observed the same
 402 trend while analyzing the phonon properties predicted by existing UO_2 empirical potentials.
 403 By including both harmonic and higher-order force constants in their phonon calculations,
 404 they found that UO_2 empirical potentials that overestimate the 0 K optical phonon frequency
 405 range tend to underestimate the specific heat, especially at near-melting temperatures. Zhou
 406 *et al.* [85] also made a similar observation about the Stillinger-Weber potential of GaN, and
 407 attributed its underestimation of the specific heat at high temperatures to the overestimated
 408 optical phonon range. The Debye temperature quantifies the temperature above which all
 409 phonon modes become excited and below which some phonon modes freeze out [86]. Based
 410 on our analysis in Section 3.3, θ_D is around 362 K, which means that even at temperatures
 411 near RT we can expect optical phonons to contribute to the UN specific heat. Baranov *et al.*
 412 [81] also noted that due to the ionic character of the UN chemical bond, optical phonons are
 413 expected to predominate the oscillation spectrum of the UN lattice at temperatures above
 414 θ_D .

415 The agreement between the lattice thermal conductivity predicted by Galvin *et al.* [71]

416 using both potentials despite the discrepancy of the predicted specific heats can be under-
417 stood if we note that the two potentials predict the same acoustic phonon spectrum and DOS
418 at 0 K. For bulk materials, the thermal conductivity is largely dictated by acoustic phonons
419 because they are the main heat carriers [87]. In contrast, the contribution of optical phonons
420 to the thermal conductivity of bulk materials is very small due to their short lifetimes and
421 low group velocities [88].

422 *3.6. Point defect formation energies*

423 Perfect $6 \times 6 \times 6$ supercells of UN were energy-minimized at 0 K using the conjugate
424 gradient algorithm implemented in LAMMPS. A fractional energy tolerance of 1×10^{-9} was
425 used allowing volume change. For the Tseplyaev potential, we used energy tolerances in the
426 range 10^{-6} - 10^{-15} and found that the raw formation energies of the defective supercells vary by
427 several eV with decreasing the energy tolerance down to a tolerance of 10^{-9} at which the raw
428 formation energy becomes somewhat insensitive to the energy tolerance. This is indicative
429 of the complex potential energy surface predicted by the Tseplyaev potential and the likely
430 existence of several metastable states. This strong dependence of the raw formation energy
431 on energy tolerance was not observed for the Kocevski potential. The cohesive energies
432 of UN, α -U, and UN_2 and chemical potentials were calculated for both potentials and are
433 shown in [Tables B.7](#) and [B.8](#). It should be noted that the Kocevski potential predicts
434 positive cohesive energy for α -U (i.e., it cannot predict a stable α -U phase), which would
435 lead to unphysical chemical potentials and incorrect formation energies for the U-rich and
436 stoichiometric conditions. For this reason, point defects under U-rich and stoichiometric
437 conditions are not considered for the Kocevski potential in this work.

438 For the 0 K calculations, point defects were then introduced into $6 \times 6 \times 6$ UN supercells.
439 U and N interstitials were inserted only in cubic interstitial sites. Yang and Kaltsoyannis
440 [[19](#)] have observed that when a U Frenkel defect is introduced within a UN supercell, it is
441 annihilated by the tiny atomic movements of the relaxation process. To prevent this phe-
442 nomenon, the initial forces on all inserted interstitials were set to zero. Defective supercells
443 were relaxed using the same procedure used for the perfect supercells.

444 To avoid the possibility of defective supercells converging to metastable energy states
445 by static minimization at 0 K, the 0 K formation energies are averaged over many defect
446 configurations, and, additionally, the formation energies are also calculated at 1 K. $8 \times 8 \times 8$
447 supercells of UN are equilibrated in the *NPT* ensemble for 50 ps, where the system's potential
448 energy is averaged over the last 20 ps. Point defects are inserted in the equilibrated UN
449 supercells, and the defective system is allowed to evolve under the *NPT* ensemble for 50 ps
450 where the system's potential energy is also averaged over the last 20 ps. The calculation is
451 repeated using five unique initial velocity distributions, utilizing the average potential energy
452 of this sample to obtain defect energetics. Chemical potentials and formation energies are
453 calculated using the same procedure employed at 0 K. The Tseplyaev potential is also used to
454 calculate the finite-temperature formation enthalpy for U FD, N FD, and SD with 15 unique
455 initial velocity distributions in the temperature range of 100-1500 K. The 1500 K limit is
456 chosen because in UN diffusion begins to be experimentally observed at this temperature
457 [[89](#)]. Thus, at and beyond 1500 K, the measured raw formation enthalpies would be affected
458 by defect migration.

Table 3: Formation energies (eV) for stoichiometric point defects. FD stands for Frenkel defect, and SD stands for Schottky defect. A [..¹⁵]semi-bound SD is composed of two vacancies at (0, 0, 0) and (0.5, 0.5, 0.5).

	Tseplyaev potential		Kocevski potential		DFT	
	0 K	1 K	0 K	1 K		
[.. ¹⁶]Unbound U FD	9.32	8.02	14.41	14.30	9.46 [19], 6.31-10.19 [10]	-
[.. ¹⁷]Bound U FD	7.26	-	10.3	-	-	-
[.. ¹⁸]Unbound N FD	4.67	4.50	4.03	4.00	4.90-5.04 [19], 4.43-4.95 [10]	-
[.. ¹⁹]Bound N FD	3.76	-	3.23	-	-	-
[.. ²⁰]Unbound SD	4.57	4.52	3.98	3.88	4.96-5.15 [19], 4.25-5.47 [10]	-
[.. ²¹]Semi-bound SD	4.51	-	3.99	-	-	-
[.. ²²]Bound SD (divacancy)	4.35	-	3.04	-	4.17 [19]	-

Table 4: Formation energies (eV) for non-stoichiometric point defects. Standard Kröger-Vink notation [90] has been used for point defects but with charges omitted due to the inability of MD to simulate charged defects.

	U-rich				Stoichiometric				N-rich			
	Tseplyaev		DFT		Tseplyaev		DFT		Tseplyaev		DFT	
	0 K	1 K			0 K	1 K			0 K	1 K		
[.. ²³] V_U	3.45	3.33	3.17-3.43 [19], 3.27-3.86 [10]	2.19	2.14	2.75-3.01 [19]	0.93	0.95	0.60	0.54	2.34-2.60 [19], 2.09-2.58 [10]	-
[.. ²⁴] V_N	1.11	1.29	1.76-1.90 [19], 0.62-1.86 [10]	2.37	2.48	2.18-2.31 [19]	3.62	3.67	3.35	3.34	2.59-2.72 [19], 1.42-2.82 [10]	-
[.. ²⁵] U_i	6.43	3.99	2.81-6.33 [10]	7.69	5.18	-	8.95	6.37	13.82	13.76	3.79-7.78 [10]	-
[.. ²⁶] N_i	3.73	3.21	2.96-3.82 [10]	2.47	2.02	-	1.21	0.83	0.89	0.66	2.00-3.01 [10]	-
[.. ²⁷] U_N	1.61	1.86	1.74-3.16 [10]	4.13	4.24	-	6.65	6.62	18.32	15.90	3.72-5.52 [10]	-
[.. ²⁸] N_U	9.32	5.84	5.99-7.67 [10]	6.80	3.46	-	4.28	1.08	4.71	1.70	4.06-5.19 [10]	-

The calculated formation energies are reported in Tables 3 and 4. [..²⁹]Bound SD and FD are formed by introducing the two vacancies, and the vacancy and interstitial, respectively, within the same unit cell, whereas [..³⁰]unbound SD and FD are formed by introducing the two vacancies, and the vacancy and interstitial, respectively, within different unit cells. Dashes in Table 3 for [..³¹]bound defects at 1 K indicate that these defects relaxed to the defect-free crystal structure. The formation energy of the N FD is slightly higher than the formation energies of the [..³²]unbound SD and divacancy due to the lattice's compact structure which offers limited room for an interstitial. The formation energies predicted by the Tseplyaev potential at 0 K and 1 K are generally consistent with each other except for the values predicted for [..³³]unbound U FD, [..³⁴] U_i , and N_U which show differences in the range 1.30-3.48 eV, with the 0 K values being generally larger than the 1 K values. This is because calculating the formation energies at 1 K using the Tseplyaev potential allows us to approach the ground state of the defect structure, whereas the calculation at 0 K fails to do so. This is especially true for [..³⁵] U_i , whose most stable configuration in UN is reported as the dumbbell configuration [24], whereas, by visual inspection of the [..³⁶] U_i

²⁹removed: Bonded

³⁰removed: unbonded

³¹removed: bonded

³²removed: unbonded

³³removed: unbonded

³⁴removed: U_i , and N_U

³⁵removed: U_i

³⁶removed: U_i

474 structure at 0 K (not shown), [..³⁷] U_i still resides at the cubic interstitial site after static
 475 minimization using the Tseplyaev potential. The difference in [..³⁸] U_i formation energy
 476 between 0 K and 1 K also explains the difference in the formation energy of U FD. This
 477 discrepancy most likely signifies that the Tseplyaev potential predicts metastable states for
 478 the defected UN supercells at 0 K, a situation that we also encountered with strained UN
 479 supercells at 0 K. Thus, caution should be exercised when utilizing or examining 0 K defect
 480 properties calculated by the Tseplyaev potential. The formation energies predicted by the
 481 Tseplyaev potential generally show excellent agreement with the DFT-predicted values for
 482 U-rich, N-rich, and stoichiometric conditions. The Kocevski potential predicts formation
 483 energies for N FD and SD in agreement with DFT, but it overestimates the U FD defect by
 484 more than 4 eV. As explained previously, the Kocevski potential cannot predict formation
 485 energies for U-rich and stoichiometric conditions due to the inability to describe metallic U.
 486 However, for N-rich conditions, the formation energies predicted by the Kocevski potential
 487 qualitatively agree with DFT-values for most defects except for [..³⁹] U_i and U_N , which are
 488 overestimated by a factor of 2-3. It can be concluded that the Tseplyaev potential shows a
 489 better performance in the calculation of point defect formation energy, whereas the Kocevski
 490 potential is only suitable for stoichiometric point defects. It can also be concluded that [..⁴⁰
 491], in [..⁴¹] UN, hypo-stoichiometry is accommodated by V_N and U_N , whereas hyper-stoichiometry
 492 is accommodated by V_U and N_i .

493 Lastly, it is interesting to note that the formation energy of U_N at 1 K is nearly one-half of its
 494 value at 0 K for all cases. Based on visual inspection it was noticed that the following reaction
 495 takes place:



496 where $NN-D\langle 111 \rangle$ refers to the N-N dumbbell along the $\langle 111 \rangle$ direction. This reaction likely leads
 497 to a reduction in the formation energy. Although Kuksin *et al.* [24] did not consider N_U they
 498 reported similar reactions for other defect types in UN as well as uranium monocarbide (UC).

499 Formation enthalpies of U FD, N FD, and SD in UN as a function of temperature are
 500 shown in Fig. 6. As expected, the standard deviation increases with increasing temperature.
 501 The average formation enthalpy of U FD is confined to about 7-8 eV, whereas those of N
 502 FD and SD are confined to about 4-5 eV, with no apparent dependence on temperature.

503 3.7. UN_2 , α - U_2N_3 and β - U_2N_3

504 3.7.1. Thermophysical properties

505 The UN_2 lattice parameter and C_P predicted by both potentials are shown in Figs. 7a
 506 and 7b, respectively. The Tseplyaev potential gives a better prediction of the UN_2 lattice
 507 parameter with a slight underestimation and predicts a phase transition at about 800 K. On
 508 the other hand, the Kocevski potential overestimates the UN_2 lattice parameter and predicts
 509 a stable UN_2 crystal structure up to 1400 K. It should be noted that the phase transition

³⁷removed: U_i

³⁸removed: U_i

³⁹removed: U_i and U_N

⁴⁰removed: in U-rich conditions, V_N and U_N accommodate most of the off-stoichiometry, whereas

⁴¹removed: N-rich conditions, V_U and N_i accommodate most of the off-stoichiometry.

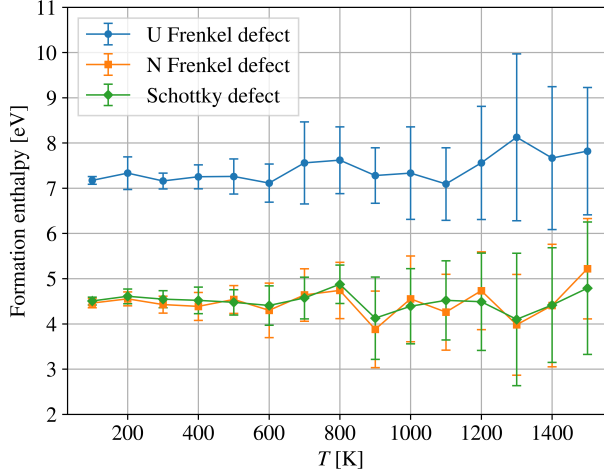


Figure 6: Defect formation enthalpy as a function of temperature for the **unbound** U Frenkel defect, **unbound** N Frenkel defect, and **unbound** Schottky defect in UN as a function of temperature as calculated by the Tseplyaev potential. Error bars correspond to one standard deviation.

temperature of UN_2 is 1324–1405 K [4, 38]. It is also worth mentioning that Silva *et al.* [31] reported lattice constants of UN_2 and $\alpha\text{-U}_2\text{N}_3$ as a function of temperature; however, their samples were not of high purity but rather included the $\text{UN}_2/\alpha\text{-U}_2\text{N}_3$ solid solution, and, thus, are not ideal for comparison. The Tseplyaev potential overestimates the $\text{UN}_2 C_P$ compared to that calculated by the Kocevski potential, a trend that was also observed for UN. Due to the lack of experimental measurements, we compare the predicted C_P with the Dulong–Petit value which, for a compound, is defined as $3nR$, n being the number of atoms per formula unit ($n = 3$ for UN_2 , and $n = 5$ for α - and $\beta\text{-U}_2\text{N}_3$), and R being the gas constant [91]. The Dulong–Petit value serves as a theoretical lower limit on C_P data for solids well above room temperature and is useful to compare against in the absence of experimental measurements. The $\text{UN}_2 C_P$ predicted by both potentials approach the Dulong–Petit value around room temperature and deviate from it at higher temperatures, which is the theoretically expected trend [..⁴²] [86]. In general, the specific heat reaches the Dulong-Petit value at temperatures near and below room temperature because of the inability of MD simulations to model the quantum effects that would otherwise lead to the decrease of specific heat with temperature up to 0 K according to the Debye model [86]. Thus, the classical thermodynamic Dulong-Petit value holds at low temperatures. However, at high temperatures, the specific heat is swamped by phonon dynamics which can be modeled by MD to some level of accuracy.

The Tseplyaev potential could not predict a stable **crystal** structure above 0 K for either $\alpha\text{-U}_2\text{N}_3$ or $\beta\text{-U}_2\text{N}_3$, so we only discuss the finite temperature α - and $\beta\text{-U}_2\text{N}_3$ properties predicted by the Kocevski potential (Fig. B.11). The Kocevski potential predicts that the $\alpha\text{-U}_2\text{N}_3$ phase is [..⁴³] has a stable crystal structure up to about 1000 K. For $\alpha\text{-U}_2\text{N}_3$, the Kocevski potential overestimates the lattice parameter, and for $\beta\text{-U}_2\text{N}_3$, it overestimates

⁴²removed: .

⁴³removed: mechanically stable

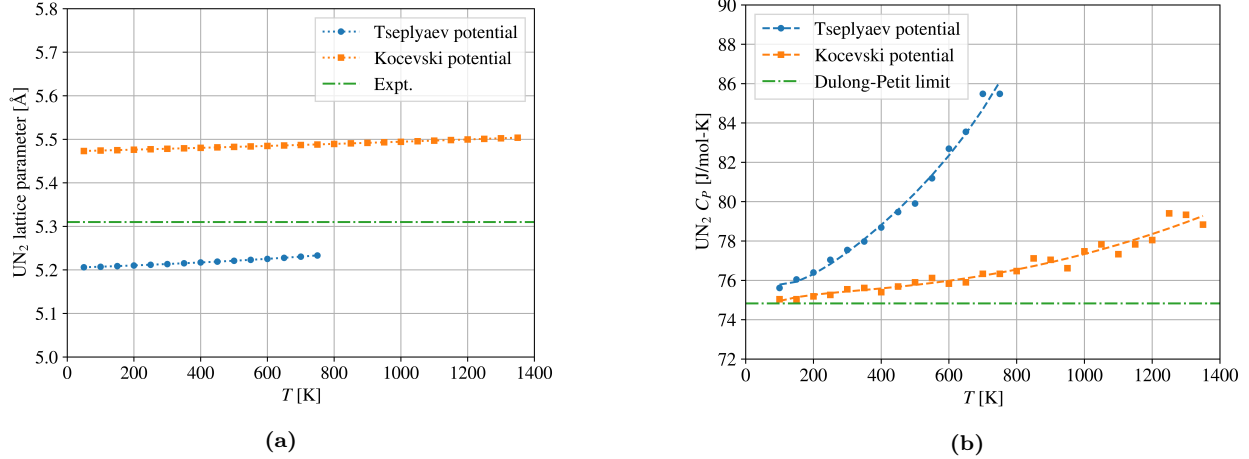


Figure 7: (a) The lattice parameter of UN₂ calculated by both potentials as a function of temperature. (b) UN₂ C_P calculated by both potentials as a function of temperature. C_P calculated by the Tseplyaev and Kocevski potentials are fitted to Eqs. (B.9) and (B.10), respectively. The experimental lattice parameter of UN₂ is taken from Lu *et al.* [92] and included as a horizontal line because the temperature at which it was measured is not reported.

the a parameter and underestimates the c parameter. The α - and β -U₂N₃ C_P predicted by the Kocevski potential nearly coincide and approach the Dulong–Petit value around RT. Additionally, the Kocevski potential predicts that the β -U₂N₃ crystal structure can be [...] stabilized at very low temperatures.

As mentioned earlier, the Tseplyaev potential is a modified version of the ADP developed by Kuskin *et al.* [24]. The authors reported that Kuksin’s potential could stabilize the crystal structures of α - and β -U₂N₃. However, Tseplyaev and Starikov [25] don’t report any capability of the modified version of the potential to simulate polymorphs of U₂N₃ at zero pressure. Thus, it appears that in the modification of the potential to improve UN property prediction, the capability was lost for other phases in the U-N system.

3.7.2. Elastic properties

The 0 K elastic constants of UN₂ are shown in Table 5. The predictions of the Kocevski potential show a good agreement with the DFT predictions for C_{12} and C_{44} , whereas it underestimates C_{11} by about 40%. The predictions of the Tseplyaev potential show much larger errors: it overestimates C_{11} and C_{12} by more than 70%, and 40%, respectively, and its C_{44} value is overestimated by nearly a factor of 5. The temperature dependence of the UN₂ elastic constants and moduli are shown in Fig. 8. The Kocevski potential shows general qualitative agreement with the UN₂ elastic moduli predicted by DFT, whereas the Tseplyaev potential greatly overestimates all elastic moduli and fails to give qualitative predictions. The Kocevski potential shows minimal softening of the UN₂ elastic properties with increasing temperature.

The 0 K elastic constants of α -U₂N₃ calculated by the Kocevski potential are $C_{11} = 185.4$ GPa, $C_{22} = 141.8$ GPa, and $C_{44} = 41.8$ GPa, whereas the elastic constants and

⁴⁴removed: mechanically stable

Table 5: UN_2 elastic constants (GPa) at 0 K as calculated by both potentials. The DFT values are from Lu *et al.* [92] and have been calculated using the GGA+ U approach with $U = 2$ eV.

	C_{11}	C_{12}	C_{44}
Tseplyaev potential	856.2	201.4	291.7
Kocevski potential	275.9	184.1	67.8
DFT [92]	488.2	140.5	55.3

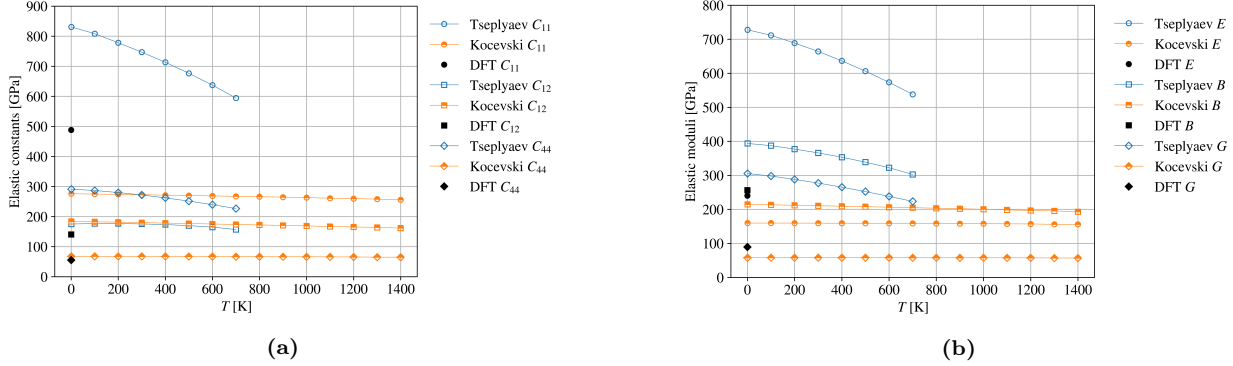


Figure 8: The predicted temperature variation of (a) UN_2 elastic constants, C_{11} , C_{12} , and C_{44} , (b) UN_2 Young's modulus, E , bulk modulus, B , and shear modulus, G . The DFT values are from Lu *et al.* [92].

moduli calculated at finite temperatures are shown in Figs. 9a and 9b, respectively. To the best of our knowledge, no experimental or DFT elastic property data exist for $\alpha\text{-U}_2\text{N}_3$. It can be observed that $\alpha\text{-U}_2\text{N}_3$ is generally softer than UN_2 which is expected because, as explained earlier, the $\alpha\text{-U}_2\text{N}_3$ conventional unit cell lacks 16 N atoms, and thus has fewer bonds compared to the $2 \times 2 \times 2$ UN_2 supercell.

For $\beta\text{-U}_2\text{N}_3$, the 0 K elastic constants are shown in Table 6. The predictions of both potentials satisfy the elastic stability criteria of the hexagonal lattice and nearly agree, except for C_{33} which the Tseplyaev potential overpredicts by a factor of 23, and C_{44} which the Tseplyaev potential underestimates with an error of about 50%—all relative to the values predicted by the Kocevski potential at 0 K. The bulk modulus predicted by the Kocevski potential agrees perfectly with that predicted by the DFT study of Lu *et al.* [92]. The elastic constants and bulk modulus of $\beta\text{-U}_2\text{N}_3$ predicted by the Tseplyaev potential vary significantly by varying the strain, whereas those predicted by the Kocevski potential show a negligible dependence on the strain value. This is indicative of potential instabilities using the Tseplyaev potential for $\beta\text{-U}_2\text{N}_3$, which are confirmed through the evaluation of the structure at finite temperatures, which decomposes as discussed. The variation of the $\beta\text{-U}_2\text{N}_3$ elastic constants with temperature is shown in Fig. 10a. C_{11} and C_{33} show observable softening, C_{12} shows a slower softening rate, and C_{13} and C_{44} are nearly constant. $\beta\text{-U}_2\text{N}_3$ elastic moduli are shown in Fig. 10b. As explained earlier, the predicted bulk modulus qualitatively agrees with DFT values. In general, further experimental investigations are required to validate the predicted properties of UN_2 , $\alpha\text{-U}_2\text{N}_3$, and $\beta\text{-U}_2\text{N}_3$.

Table 6: β -U₂N₃ elastic properties (GPa) as calculated by both potentials. $B = 232$ GPa has been calculated by Evarestov *et al.* [7] using the LCAO DFT approach. $B = 209.2$ GPa has been calculated by Lu *et al.* [92] using the GGA+ U approach with $U = 2$ eV.

	C_{11}	C_{12}	C_{13}	C_{33}	C_{44}	B
Tseplyaev potential	372.4	166.8	118.1	5680.1	30.0	534.5
Kocevski potential DFT	357.0	224.2	140.7	242.7	64.5	210.0
						232 [7], 209.2 [92]

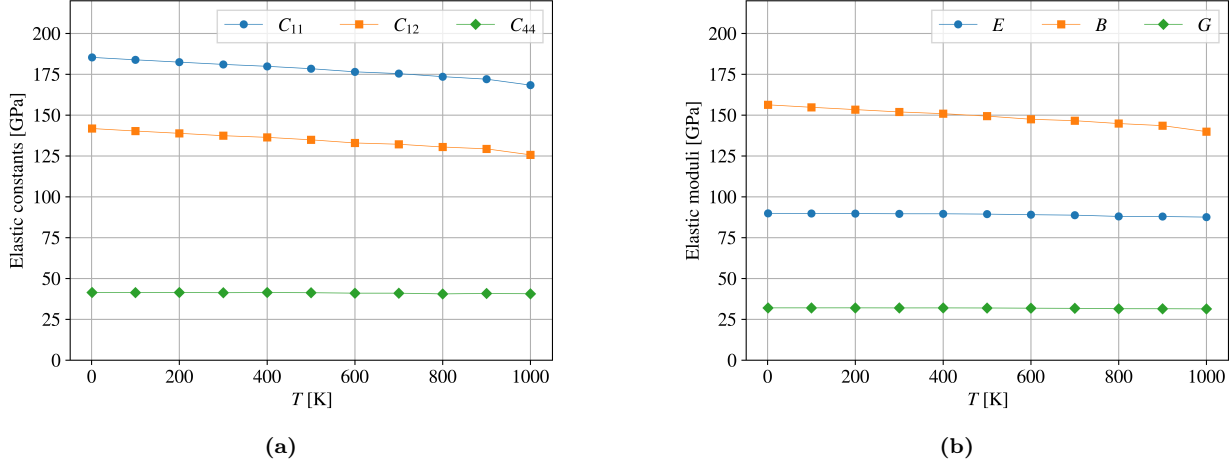


Figure 9: (a) Elastic constants, C_{11} , C_{12} , and C_{44} , (b) Young's modulus, E , bulk modulus, B , and shear modulus, G , of α -U₂N₃ as calculated by the Kocevski potential.

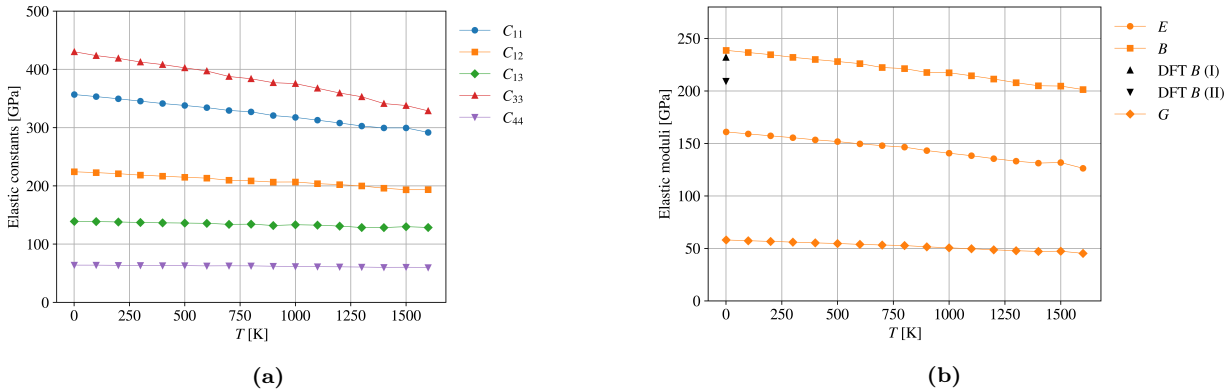


Figure 10: (a) Elastic constants, C_{11} , C_{12} , C_{13} , C_{33} , and C_{44} , (b) Young's modulus, E , bulk modulus, B , and shear modulus, G , of β -U₂N₃ as calculated by the Kocevski potential. DFT B (I) is from Evarestov *et al.* [7] and DFT B (II) is from Lu *et al.* [92].

578 4. Discussion

Based on the presented results, we can identify several features of both potentials. In general, the Kocevski potential shows better predictability of the structural aspects of UN, e.g., lattice parameter and elastic properties as a function of temperature, whereas the Tseplyaev potential better predicts the UN energetic aspects, e.g., the specific heat and defect formation energies. One drawback of the Kocevski potential is the overestimation of the UN optical phonon range, leading to its underestimation of the UN C_P , compared

585 to the Hayes *et al.* [33] correlation, at temperatures greater than 1200 K. Moreover, the
586 Kocevski potential cannot predict a stable metallic α -U structure. Therefore, its applicability
587 to studies related to UN non-stoichiometry is limited. The Tseplyaev potential does an
588 inferior job of predicting the UN elastic properties and underpredicts the experimental lattice
589 parameter values compared to the Kocevski potential. The Tseplyaev potential predicts [..⁴⁵
590]the UN phonon band structure [..⁴⁶]with reasonable accuracy, which makes it preferable
591 in the evaluation of thermal conductivities. Another important feature of the Tseplyaev
592 potential is that it predicts metastable states for defected UN supercells at 0 K, and thus
593 we recommend avoiding its usage at 0 K. Thus, each potential has realms of applicability
594 for the description of the UN system, and the noted drawbacks must be acknowledged when
595 deciding which potential to utilize.

596 The predictions of UN_2 properties by the Kocevski potential show better qualitative
597 agreement with the limited experimental and DFT values; however, neither potential pro-
598 duces results with a satisfactory level of accuracy. The Tseplyaev potential cannot predict
599 stable structures for α - and β - U_2N_3 and predicts premature phase change of both UN and
600 UN_2 . Thus, the Tseplyaev potential is not suitable for studies related to the stability of
601 different uranium nitride phases. On the other hand, the Kocevski potential predicts stable
602 α - and β - U_2N_3 structures with reasonable lattice parameters, reasonably predicts the melt-
603 ing point of UN and predicts a [..⁴⁷]crystal structure stability range of UN_2 closer to that
604 represented by the U-N system phase diagrams. This makes the Kocevski potential the best
605 option for studies involving many uranium nitride phases, although more experimental data
606 are needed to further assess its predictions of UN_2 , and α - and β - U_2N_3 properties.

607 Areas of importance that have not been assessed in this study include the dynamical pro-
608 cesses of plastic deformation, i.e., dislocation formation and slip, interfacial properties, and
609 radiation damage. Such analyses are beyond the scope of this work, but potential compari-
610 son and validation should be conducted before utilization of either potential to explore these
611 phenomena. Another interesting aspect worth exploring in future studies is the high-pressure
612 phase transition that UN undergoes from the cubic $Fm\bar{3}m$ structure to the rhombohedral $R\bar{3}m$
613 structure [93, 94, 9]. Experimentally, this transition was observed to occur at 29 GPa [93], and
614 the Tseplyaev potential predicted it to take place at a pressure of 35 GPa [25]. However, the
615 Kocevski potential was never used to study this aspect.

616 5. Conclusions

617 This work aimed to evaluate two UN interatomic potentials: Tseplyaev and Starikov's
618 ADP [25] and Kocevski *et al.*'s EAM potential [27]. The study involved assessing the pre-
619 dictive capabilities of these potentials for various thermophysical and elastic properties of
620 UN, UN_2 , and α - and β - U_2N_3 . The Kocevski potential underestimates the UN specific heat
621 which is attributed to its overestimation of the UN optical phonon frequency range. In terms

⁴⁵removed: with reasonable accuracy

⁴⁶removed: , although the predicted optical branches coincide near the Γ -point due to the absence of long-
range electrostatic interactions in the ADP model. The relative accuracy of the phonon behavior predicted
by the Tseplyaev potential should make

⁴⁷removed: mechanical

622 of performance, the Tseplyaev potential excels in capturing the energetic aspects of UN,
 623 whereas the Kocevski potential performs better in modeling the UN's structural properties.
 624 Regarding the [..⁴⁸] crystal structure stability of phases, the Kocevski potential demonstrates
 625 superior predictive capabilities, in that it can reasonably estimate the UN melting point
 626 and predicts stable α - and β -U₂N₃ structures. In contrast, the Tseplyaev potential predicts
 627 premature phase changes for both UN and UN₂ and fails to stabilize either polymorph of
 628 U₂N₃. An important limitation of the Kocevski potential is its inability to predict a stable
 629 metallic U phase, making it unsuitable for studies related to UN non-stoichiometry.

630 Acknowledgements

631 The authors would like to thank Antoine Claisse for the fruitful discussions. Mohamed
 632 AbdulHameed dedicates this work to the memory of Abu Bakr Etman. This research made
 633 use of the resources of the High-Performance Computing Center at Idaho National Labora-
 634 tory, which is supported by the Office of Nuclear Energy of the U.S. Department of Energy
 635 and the Nuclear Science User Facilities under Contract No. DE-AC07-05ID14517.

636 Appendix A. Voigt-Reuss-Hill elastic moduli

637 For an isotropic polycrystalline material with a cubic crystal structure, the form of the
 638 VRH elastic moduli is [46, 95]:

$$B = B_V = B_R = \frac{C_{11} + 2C_{12}}{3} \quad (\text{A.1})$$

$$G_V = \frac{C_{11} - C_{12} + 3C_{44}}{5} \quad (\text{A.2})$$

$$G_R = \frac{5C_{44}(C_{11} - C_{12})}{4C_{44} + 3(C_{11} - C_{12})} \quad (\text{A.3})$$

$$G = \frac{G_V + G_R}{2} \quad (\text{A.4})$$

$$E = \frac{9BG}{3B + G} \quad (\text{A.5})$$

$$\nu = \frac{3B - 2G}{6B + 2G} \quad (\text{A.6})$$

639 For the β -U₂N₃ hexagonal crystal, the Voigt and Reuss limits on the bulk and shear
 640 moduli are formulated in terms of the components of both the stiffness tensor, C_{ij} , and the
 641 compliance tensor, S_{ij} [46, 96]:

$$B_V = \frac{2C_{11} + 2C_{12} + 4C_{13} + C_{33}}{9} \quad (\text{A.7})$$

⁴⁸removed: mechanical

642

$$B_R = \frac{1}{2S_{11} + 2S_{12} + 4S_{13} + S_{33}} \quad (\text{A.8})$$

643

$$B = \frac{B_V + B_R}{2} \quad (\text{A.9})$$

644

$$G_V = \frac{2C_{11} - C_{12} - 2C_{13} + C_{33} + 6C_{44} + 3C_{66}}{15} \quad (\text{A.10})$$

645

$$G_R = \frac{15}{8S_{11} - 4S_{12} - 8S_{13} + 4S_{33} + 6S_{44} + 3S_{66}} \quad (\text{A.11})$$

where S_{11} , S_{12} , S_{13} , S_{33} , and S_{44} are the independent components of the compliance tensor, and:

$$S_{11} = \frac{C_{11}C_{33} - C_{13}^2}{C_{11}(C_{11}C_{33} - 2C_{13}^2) - C_{12}(C_{12}C_{33} + 2C_{13}^2)} \quad (\text{A.12})$$

648

$$S_{12} = \frac{-C_{12}C_{33} + C_{13}^2}{C_{11}(C_{11}C_{33} - 2C_{13}^2) - C_{12}(C_{12}C_{33} + 2C_{13}^2)} \quad (\text{A.13})$$

649

$$S_{13} = \frac{-C_{13}}{C_{33}(C_{11} + C_{12}) - 2C_{13}^2} \quad (\text{A.14})$$

650

$$S_{33} = \frac{C_{11} + C_{12}}{C_{33}(C_{11} + C_{12}) - 2C_{13}^2} \quad (\text{A.15})$$

651

$$S_{44} = \frac{1}{C_{44}} \quad (\text{A.16})$$

652

$$C_{66} = \frac{C_{11} - C_{12}}{2} \quad (\text{A.17})$$

653

$$S_{66} = 2(S_{11} - S_{12}) \quad (\text{A.18})$$

Appendix B. Supplementary information

In all equations presented in this appendix, the superscript T refers to the Tseplyaev potential and the superscript K refers to the Kocevski potential.

The temperature variation of the LTEC computed by both potentials is fitted to the following functions:

$$\alpha_L^T = 7.321 \times 10^{-6} - 3.063 \times 10^{-11}T + 2.154 \times 10^{23}T^5 \quad (R^2 = 99.8\%) \quad (\text{B.1})$$

659

$$\alpha_L^K = 5.773 \times 10^{-6} + 3.866 \times 10^{-10}T + 1.813 \times 10^{-13}T^2 \quad (R^2 = 99.9\%) \quad (\text{B.2})$$

in the temperature range 50-2500 K.

The temperature dependence of the bulk modulus computed by both potentials is fitted to the following quadratic functions:

$$B^T = 275.063 - 3.314 \times 10^{-2}T - 7.649 \times 10^{-6}T^2 \quad (R^2 = 98.4\%) \quad (\text{B.3})$$

663

$$B^K = 219.196 - 1.955 \times 10^{-2}T - 4.517 \times 10^{-6}T^2 \quad (R^2 = 99.8\%) \quad (\text{B.4})$$

in the temperature range of 1-2600 K.

665 The UN C_P and C_V computed by both potentials have been fitted to:

$$C_P^T = 61.612 + 4.709 \times 10^{-3}T + 3.754 \times 10^{-16}T^5 - 19.663/T^{0.1} \quad (R^2 = 99.4\%) \quad (\text{B.5})$$

$$C_P^K = 50.500 + 6.193 \times 10^{-3}T + 1.272 \times 10^{-13}T^4 - 1.140/T^{0.1} \quad (R^2 = 99.7\%) \quad (\text{B.6})$$

$$C_V^T = 49.341 + 7.144 \times 10^{-4}T + 4.016 \times 10^{-8}T^{2.5} + 0.591/T^{0.1} \quad (R^2 = 98.8\%) \quad (\text{B.7})$$

$$C_V^K = 49.978 + 8.757 \times 10^{-4}T + 1.616 \times 10^{-7}T^2 \quad (R^2 = 80.8\%) \quad (\text{B.8})$$

666 The UN₂ C_P calculated by both potentials are fitted to:

$$C_P^T = 54.894 + 1.803 \times 10^{-2}T + 8.717 \times 10^{-15}T^5 + 30.248/T^{0.1} \quad (R^2 = 98.9\%) \quad (\text{B.9})$$

$$C_P^K = 82.060 - 2.445 \times 10^{-3}T + 3.199 \times 10^{-6}T^2 - 10.934/T^{0.1} \quad (R^2 = 95.1\%) \quad (\text{B.10})$$

667 whereas the α -U₂N₃ C_P calculated by the Kocevski potential is fitted to:

$$C_P^K = 155.092 - 1.686 \times 10^{-2}T + 1.534 \times 10^{-5}T^2 - 45.235/T^{0.1} \quad (R^2 = 93.3\%) \quad (\text{B.11})$$

668 and the β -U₂N₃ C_P calculated by the Kocevski potential is fitted to:

$$C_P^K = 132.240 + 7.979 \times 10^{-4}T + 2.544 \times 10^{-6}T^2 - 11.483/T^{0.1} \quad (R^2 = 91.1\%) \quad (\text{B.12})$$

Table B.7: Cohesive energies (eV) of UN, α -U and UN₂.

	Tseplyaev potential	Kocevski potential	Reference value
UN	-16.18	-13.02	-13.6 (Expt.) [7]
α -U	-5.23 (0 K); -5.37 (1 K)	-	-5.55 (Expt.) [97]
UN ₂	-24.62	-22.18	-21.5 to -17.9 (DFT) [7]

Table B.8: U and N chemical potentials (eV) for different stoichiometric conditions.

	Tseplyaev potential			Kocevski potential
	U-rich	Stoichiometric	N-rich	
μ_U	-5.23 (0 K); -5.37 (1 K)	-6.49 (0 K); -6.56 (1 K)	-7.75	-3.86
μ_N	-10.95 (0 K); -10.81 (1 K)	-9.69 (0 K); -9.62 (1 K)	-8.43	-9.16

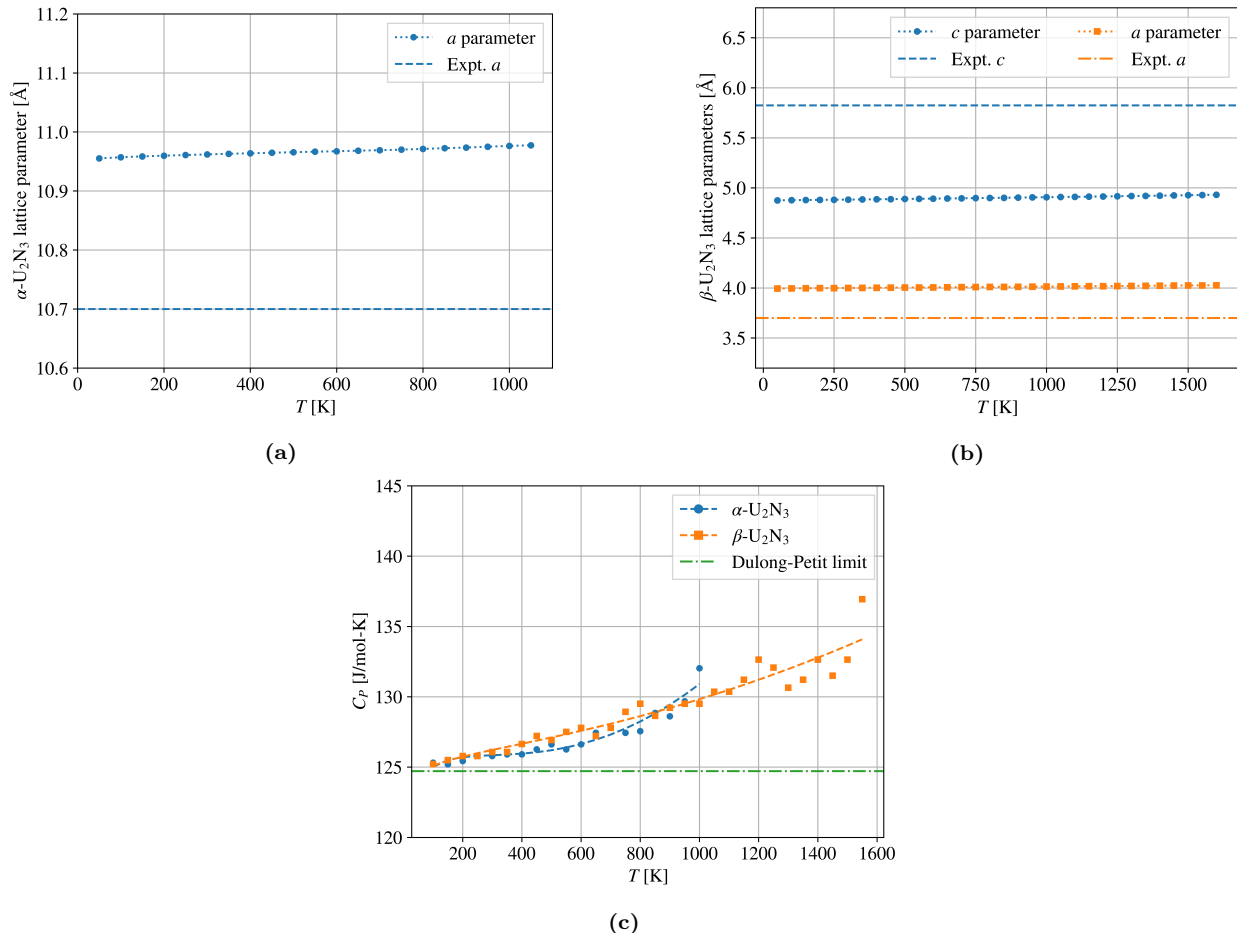


Figure B.11: The lattice parameters of (a) $\alpha\text{-U}_2\text{N}_3$, and (b) $\beta\text{-U}_2\text{N}_3$ as calculated by the Kocevski potential. (c) The specific heats of α - and $\beta\text{-U}_2\text{N}_3$ as calculated by the Kocevski potential. The curve fit of C_p of α - and $\beta\text{-U}_2\text{N}_3$ as functions of temperature are given in Eqs. (B.11) and (B.12).

669 References

- 670 [1] J. K. Watkins, A. Gonzales, A. R. Wagner, E. S. Sooby, B. J. Jaques, Challenges
671 and opportunities to alloyed and composite fuel architectures to mitigate high uranium
672 density fuel oxidation: Uranium mononitride, Journal of Nuclear Materials 553 (2021).
673 [doi:10.1016/j.jnucmat.2021.153048](https://doi.org/10.1016/j.jnucmat.2021.153048).
- 674 [2] C. Ekberg, D. R. Costa, M. Hedberg, M. Jolkkonen, Nitride fuel for Gen IV nuclear
675 power systems, Journal of Radioanalytical and Nuclear Chemistry 318 (2018) 1713–
676 1725. [doi:10.1007/s10967-018-6316-0](https://doi.org/10.1007/s10967-018-6316-0).
- 677 [3] J. Wallenius, Nitride fuels, Comprehensive Nuclear Materials 5 (2020) 88–101. [doi:
678 10.1016/B978-0-12-803581-8.11694-7](https://doi.org/10.1016/B978-0-12-803581-8.11694-7).
- 679 [4] M. Uno, T. Nishi, M. Takano, Thermodynamic and thermophysical properties of
680 the actinide nitrides, Comprehensive Nuclear Materials: Second Edition (2020) 202–
681 231[doi:10.1016/B978-0-12-803581-8.11749-7](https://doi.org/10.1016/B978-0-12-803581-8.11749-7).

- [5] A. Casagranda, L. K. Aagesen, J.-H. Ke, W. Jiang, J. D. Hales, A. Toptan, K. A. Gamble, X.-Y. Liu, S. R. Novascone, C. Matthews, D. S. Stafford, Summary of BISON milestones: NEAMS FY-20 report, Tech. rep., Idaho National Laboratory (2020).
- [6] M. Samsel-Czekała, E. Talik, P. De, R. Troć, H. Misiorak, C. Sułkowski, Electronic structure and magnetic and transport properties of single-crystalline UN, Physical Review B 76 (2007) 144426. [doi:10.1103/PhysRevB.76.144426](https://doi.org/10.1103/PhysRevB.76.144426).
- [7] R. A. Evarestov, A. I. Panin, A. V. Bandura, M. V. Losev, Electronic structure of crystalline uranium nitrides UN, U₂N₃ and UN₂: LCAO calculations with the basis set optimization, Journal of Physics: Conference Series 117 (2008). [doi:10.1088/1742-6596/117/1/012015](https://doi.org/10.1088/1742-6596/117/1/012015).
- [8] D. Gryaznov, E. Heifets, E. Kotomin, The first-principles treatment of the electron-correlation and spin-orbital effects in uranium mononitride nuclear fuels, Physical Chemistry Chemical Physics 14 (2012) 4482–4490. [doi:10.1039/c2cp40297a](https://doi.org/10.1039/c2cp40297a).
- [9] Z. G. Mei, M. Stan, B. Pichler, First-principles study of structural, elastic, electronic, vibrational and thermodynamic properties of UN, Journal of Nuclear Materials 440 (2013) 63–69. [doi:10.1016/j.jnucmat.2013.04.058](https://doi.org/10.1016/j.jnucmat.2013.04.058).
- [10] V. Kocevski, D. A. Rehn, M. W. D. Cooper, D. A. Andersson, First-principles investigation of uranium mononitride (UN): Effect of magnetic ordering, spin-orbit interactions and exchange correlation functional, Journal of Nuclear Materials 559 (2022). [doi:10.1016/j.jnucmat.2021.153401](https://doi.org/10.1016/j.jnucmat.2021.153401).
- [11] E. A. Kotomin, R. W. Grimes, Y. Mastrikov, N. J. Ashley, Atomic scale DFT simulations of point defects in uranium nitride, Journal of Physics Condensed Matter 19 (2007). [doi:10.1088/0953-8984/19/10/106208](https://doi.org/10.1088/0953-8984/19/10/106208).
- [12] E. A. Kotomin, Y. A. Mastrikov, S. N. Rashkeev, P. V. Uffelen, Implementing first-principles calculations of defect migration in a fuel performance code for UN simulations, Journal of Nuclear Materials 393 (2009) 292–299. [doi:10.1016/j.jnucmat.2009.06.016](https://doi.org/10.1016/j.jnucmat.2009.06.016).
- [13] D. Bocharov, D. Gryaznov, Y. F. Zhukovskii, E. A. Kotomin, DFT calculations of point defects on UN(001) surface, Surface Science 605 (2011) 396–400. [doi:10.1016/j.susc.2010.11.007](https://doi.org/10.1016/j.susc.2010.11.007).
- [14] J. H. Lan, Z. C. Zhao, Q. Wu, Y. L. Zhao, Z. F. Chai, W. Q. Shi, First-principles DFT+U modeling of defect behaviors in anti-ferromagnetic uranium mononitride, Journal of Applied Physics 114 (2013). [doi:10.1063/1.4846217](https://doi.org/10.1063/1.4846217).
- [15] E. A. Kotomin, Y. A. Mastrikov, First principles modeling of oxygen impurities in UN nuclear fuels, Journal of Nuclear Materials 377 (2008) 492–495. [doi:10.1016/j.jnucmat.2008.04.015](https://doi.org/10.1016/j.jnucmat.2008.04.015).

- [16] M. Klipfel, P. V. Uffelen, Ab initio modelling of volatile fission products in uranium mononitride, *Journal of Nuclear Materials* 422 (2012) 137–142. [doi:10.1016/j.jnucmat.2011.12.018](https://doi.org/10.1016/j.jnucmat.2011.12.018).
- [17] A. Claisse, M. Klipfel, N. Lindbom, M. Freyss, P. Olsson, GGA+*U* study of uranium mononitride: A comparison of the U-ramping and occupation matrix schemes and incorporation energies of fission products, *Journal of Nuclear Materials* 478 (2016) 119–124. [doi:10.1016/j.jnucmat.2016.06.007](https://doi.org/10.1016/j.jnucmat.2016.06.007).
- [18] Y. J. Zhang, J. H. Lan, C. Z. Wang, Q. Y. Wu, T. Bo, Z. F. Chai, W. Q. Shi, Theoretical investigation on incorporation and diffusion properties of Xe in uranium mononitride, *Journal of Physical Chemistry C* 119 (2015) 5783–5789. [doi:10.1021/jp510219a](https://doi.org/10.1021/jp510219a).
- [19] L. Yang, N. Kaltsoyannis, Incorporation of Kr and Xe in uranium mononitride: A density functional theory study, *Journal of Physical Chemistry C* 125 (2021) 26999–27008. [doi:10.1021/acs.jpcc.1c08523](https://doi.org/10.1021/acs.jpcc.1c08523).
- [20] K. Kurosaki, K. Yano, K. Yamada, M. Uno, S. Yamanaka, A molecular dynamics study of the heat capacity of uranium mononitride, *Journal of Alloys and Compounds* 297 (2000) 1–4.
- [21] K. Kurosaki, K. Yano, K. Yamada, M. Uno, S. Yamanaka, A molecular dynamics study of the thermal conductivity of uranium mononitride, *Journal of Alloys and Compounds* 311 (2000) 305–310.
- [22] P. H. Chen, X. L. Wang, X. C. Lai, G. Li, B. Y. Ao, Y. Long, Ab initio interionic potentials for UN by multiple lattice inversion, *Journal of Nuclear Materials* 404 (2010) 6–8. [doi:10.1016/j.jnucmat.2010.06.017](https://doi.org/10.1016/j.jnucmat.2010.06.017).
- [23] Y. Mishin, *Interatomic Potentials for Metals*, Springer, 2005.
- [24] A. Y. Kuksin, S. V. Starikov, D. E. Smirnova, V. I. Tseplyaev, The diffusion of point defects in uranium mononitride: Combination of DFT and atomistic simulation with novel potential, *Journal of Alloys and Compounds* 658 (2016) 385–394. [doi:10.1016/j.jallcom.2015.10.223](https://doi.org/10.1016/j.jallcom.2015.10.223).
- [25] V. I. Tseplyaev, S. V. Starikov, The atomistic simulation of pressure-induced phase transition in uranium mononitride, *Journal of Nuclear Materials* 480 (2016) 7–14. [doi:10.1016/j.jnucmat.2016.07.048](https://doi.org/10.1016/j.jnucmat.2016.07.048).
- [26] J. J. Li, S. T. Murphy, Diffusion in hypo-stoichiometric uranium mononitride, *Progress in Nuclear Energy* 142 (2021). [doi:10.1016/j.pnucene.2021.103995](https://doi.org/10.1016/j.pnucene.2021.103995).
- [27] V. Kocevski, M. W. Cooper, A. J. Claisse, D. A. Andersson, Development and application of a uranium mononitride (UN) potential: Thermomechanical properties and Xe diffusion, *Journal of Nuclear Materials* 562 (2022). [doi:10.1016/j.jnucmat.2022.153553](https://doi.org/10.1016/j.jnucmat.2022.153553).

- 754 [28] A. P. Thompson, H. M. Aktulga, R. Berger, D. S. Bolintineanu, W. M. Brown, P. S.
755 Crozier, P. J. in 't Veld, A. Kohlmeyer, S. G. Moore, T. D. Nguyen, R. Shan, M. J.
756 Stevens, J. Tranchida, C. Trott, S. J. Plimpton, Lammmps - a flexible simulation tool for
757 particle-based materials modeling at the atomic, meso, and continuum scales, Computer
758 Physics Communications 271 (2022). [doi:10.1016/j.cpc.2021.108171](https://doi.org/10.1016/j.cpc.2021.108171).
- 759 [29] A. Togo, I. Tanaka, First principles phonon calculations in materials science, Scripta
760 Materialia 108 (2015) 1–5. [doi:10.1016/j.scriptamat.2015.07.021](https://doi.org/10.1016/j.scriptamat.2015.07.021).
- 761 [30] A. Carreras, A. Togo, I. Tanaka, DynaPhoPy: A code for extracting phonon quasi-
762 particles from molecular dynamics simulations, Computer Physics Communications 221
763 (2017) 221–234. [doi:10.17632/v493dkxk8r.1](https://doi.org/10.17632/v493dkxk8r.1).
- 764 [31] G. W. Silva, C. B. Yeamans, A. P. Sattelberger, T. Hartmann, G. S. Cerefice, K. R.
765 Czerwinski, Reaction sequence and kinetics of uranium nitride decomposition, Inorganic
766 Chemistry 48 (2009). [doi:10.1021/ic901165j](https://doi.org/10.1021/ic901165j).
- 767 [32] S. L. Hayes, J. K. Thomas, K. L. Peddicord, Material property correlations for uranium
768 mononitride I. physical properties, Journal of Nuclear Materials 171 (1990) 262–270.
- 769 [33] S. L. Hayes, J. K. Thomas, K. L. Peddicord, Material property correlations for uranium
770 mononitride IV. thermodynamic properties, Journal of Nuclear Materials 171 (1990)
771 300–318.
- 772 [34] H. Tagawa, N. Masaki, X-ray and density studies of nonstoichiometric uranium
773 sesquinitride, Journal of Inorganic and Nuclear Chemistry 36 (1974). [doi:10.1016/0022-1902\(74\)80220-4](https://doi.org/10.1016/0022-1902(74)80220-4).
- 775 [35] C. E. Price, I. H. Warren, Some observations on uranium-nitrogen compounds, Inorganic
776 Chemistry 4 (1965). [doi:10.1021/ic50023a028](https://doi.org/10.1021/ic50023a028).
- 777 [36] N. Masaki, H. Tagawa, The structure of $\{\beta\text{-U}_2\text{N}_3\}$, Journal of Nuclear Materials 58
778 (1975). [doi:10.1016/0022-3115\(75\)90114-2](https://doi.org/10.1016/0022-3115(75)90114-2).
- 779 [37] D. A. Weber, C. Schwickert, A. Senyshyn, M. Lerch, R. Pöttgen, Physical properties
780 and lattice dynamics of bixbyite-type V_2O_3 , Journal of Materials Research 32 (2017).
781 [doi:10.1557/jmr.2017.144](https://doi.org/10.1557/jmr.2017.144).
- 782 [38] H. Okamoto, N-U (nitrogen-uranium), Journal of Phase Equilibria 18 (1997) 107.
- 783 [39] S. Alavi, D. L. Thompson, Simulations of melting of polyatomic solids and nanoparticles,
784 Molecular Simulation 32 (2006). [doi:10.1080/08927020600823158](https://doi.org/10.1080/08927020600823158).
- 785 [40] Y. Zhang, E. J. Maginn, A comparison of methods for melting point calculation using
786 molecular dynamics simulations, Journal of Chemical Physics 136 (2012). [doi:10.1063/1.3702587](https://doi.org/10.1063/1.3702587).
- 788 [41] F. Ercolessi, A molecular dynamics primer, Tech. rep., International Centre for Theoretical
789 Physics (1997).

- 790 [42] S. J. Blundell, K. M. Blundell, Concepts in Thermal Physics, 2nd Edition, Oxford
791 University Press, 2010.
- 792 [43] G. Clavier, N. Desbiens, E. Bourasseau, V. Lachet, N. Brusselle-Dupend, B. Rousseau,
793 Computation of elastic constants of solids using molecular simulation: comparison of
794 constant volume and constant pressure ensemble methods, Molecular Simulation 43
795 (2017) 1413–1422. [doi:10.1080/08927022.2017.1313418](https://doi.org/10.1080/08927022.2017.1313418).
- 796 [44] M. A. Meyers, K. K. Chawla, Mechanical Behavior of Materials, 2nd Edition, Cambridge
797 University Press, 2008.
- 798 [45] K. W. Böer, U. W. Pohl, Semiconductor Physics, Springer International Publishing AG,
799 2018. [doi:<https://doi.org/10.1007/978-3-319-69150-3>](https://doi.org/10.1007/978-3-319-69150-3).
- 800 [46] O. L. Anderson, A simplified method for calculating the debye temperature from elastic
801 constants, Journal of Physics and Chemistry of Solids 24 (1963) 909–917.
- 802 [47] F. Mouhat, F.-X. Coudert, Necessary and sufficient elastic stability conditions in various
803 crystal systems, Physical Review B - Condensed Matter and Materials Physics 90 (2014).
804 [doi:10.1103/PhysRevB.90.224104](https://doi.org/10.1103/PhysRevB.90.224104).
- 805 [48] D. C. Rapaport, The Art of Molecular Dynamics Simulation, 2nd Edition, Cambridge
806 University Press, 2004.
- 807 [49] H. Siethoff, K. Ahlborn, The dependence of Debye temperature on elastic constants,
808 Physica Status Solidi B 190 (1995) 179–191. [doi:10.1002/pssb.2221900126](https://doi.org/10.1002/pssb.2221900126).
- 809 [50] V. Kocevski, D. A. Rehn, A. J. Terricabras, A. van Veelen, M. W. Cooper, S. W.
810 Paisner, S. C. Vogel, J. T. White, D. A. Andersson, Finite temperature properties of
811 uranium mononitride, Journal of Nuclear Materials 576 (2023) 154241. [doi:10.1016/j.jnucmat.2023.154241](https://doi.org/10.1016/j.jnucmat.2023.154241).
- 813 [51] T. R. Pavlov, M. R. Wenman, L. Vlahovic, D. Robba, R. J. Konings, P. V. Uffelen,
814 R. W. Grimes, Measurement and interpretation of the thermo-physical properties of
815 UO_2 at high temperatures: The viral effect of oxygen defects, Acta Materialia 139
816 (2017) 138–154. [doi:10.1016/j.actamat.2017.07.060](https://doi.org/10.1016/j.actamat.2017.07.060).
- 817 [52] M. S. Bryan, J. W. Pang, B. C. Larson, A. Chernatynskiy, D. L. Abernathy, K. Gofryk,
818 M. E. Manley, Impact of anharmonicity on the vibrational entropy and specific heat of
819 UO_2 , Physical Review Materials 3 (2019). [doi:10.1103/PhysRevMaterials.3.065405](https://doi.org/10.1103/PhysRevMaterials.3.065405).
- 820 [53] R. DeHoff, Thermodynamics in Materials Science, 2nd Edition, CRC Press, 2006.
- 821 [54] E. S. R. Gopal, Specific Heats at Low Temperatures, Springer US, 1966. [doi:10.1007/978-1-4684-9081-7_4](https://doi.org/10.1007/978-1-4684-9081-7_4).
- 823 [55] J. F. Counsell, R. M. Dell, J. F. Martin, Thermodynamic properties of uranium com-
824 pounds part 2. low-temperature heat capacity and entropy of three uranium nitrides,
825 Transactions of the Faraday Society 60 (1964) 1736–1747.

- 826 [56] J. O. Scarbrough, H. L. Davis, W. Fulkerson, J. O. Betterton, Specific heat of uranium
827 mononitride from 1.3 to 4.6 K, *Physical Review* 176 (1968) 666–671.
- 828 [57] B. Szpunar, J. I. Ranasingham, J. A. Szpunar, Electronic transport of uranium mononi-
829 tride, *Journal of Modern Physics* 12 (2021). [doi:10.4236/jmp.2021.1210084](https://doi.org/10.4236/jmp.2021.1210084).
- 830 [58] F. Giustino, Materials Modelling using Density Functional Theory: Properties and
831 Predictions, 1st Edition, Oxford University Press, 2014.
- 832 [59] E. Torres, I. CheikNjifon, T. P. Kaloni, J. Pencer, A comparative analysis of the phonon
833 properties in UO_2 using the Boltzmann transport equation coupled with DFT+ U and
834 empirical potentials, *Computational Materials Science* 177 (5 2020). [doi:10.1016/j.commatsci.2020.109594](https://doi.org/10.1016/j.commatsci.2020.109594).
- 835 [60] L. T. Kong, Phonon dispersion measured directly from molecular dynamics simulations,
836 Computer Physics Communications 182 (2011). [doi:10.1016/j.cpc.2011.04.019](https://doi.org/10.1016/j.cpc.2011.04.019).
- 837 [61] A. Togo, L. Chaput, I. Tanaka, Distributions of phonon lifetimes in Brillouin zones,
838 Physical Review B - Condensed Matter and Materials Physics 91 (2015). [doi:10.1103/PhysRevB.91.094306](https://doi.org/10.1103/PhysRevB.91.094306).
- 839 [62] Y. Mishin, D. Farkas, Atomistic simulation of point defects and diffusion in B2 NiAl
840 part I. point defect energetics, *Philosophical Magazine A* 75 (1997) 169–185. [doi:10.1080/01418619708210289](https://doi.org/10.1080/01418619708210289).
- 841 [63] C. G. V. de Walle, J. Neugebauer, First-principles calculations for defects and impurities:
842 Applications to III-nitrides, *Journal of Applied Physics* 95 (2004) 3851–3879. [doi:10.1063/1.1682673](https://doi.org/10.1063/1.1682673).
- 843 [64] S. Anand, J. P. Male, C. Wolverton, G. J. Snyder, Visualizing defect energetics, *Mate-
844 rials Horizons* 8 (2021) 1966–1975. [doi:10.1039/d1mh00397f](https://doi.org/10.1039/d1mh00397f).
- 845 [65] B. Dorado, M. Freyss, G. Martin, GGA+ U study of the incorporation of iodine in
846 uranium dioxide, *The European Physical Journal B* 69 (2009) 203–209. [doi:10.1140/epjb/e2009-00145-0](https://doi.org/10.1140/epjb/e2009-00145-0).
- 847 [66] C. Freysoldt, B. Grabowski, T. Hickel, J. Neugebauer, G. Kresse, A. Janotti, C. G. V.
848 de Walle, First-principles calculations for point defects in solids, *Reviews of Modern
849 Physics* 86 (2014) 253–305. [doi:10.1103/RevModPhys.86.253](https://doi.org/10.1103/RevModPhys.86.253).
- 850 [67] M. Hagen, M. W. Finnis, Determination of the atomistic structure of the $\Sigma 3$ (111) twin
851 boundary in NiAl, *Materials Science Forum* 207-209 (1996) 245–248. [doi:10.4028/www.scientific.net/msf.207-209.245](http://www.scientific.net/msf.207-209.245).
- 852 [68] C. Woodward, S. Kajihara, L. H. Yang, Site preferences and formation energies of
853 substitutional Si, Nb, Mo, Ta, and W solid solutions in L1_0 Ti-Al, *Physical Review B*
854 57 (1998).

- 861 [69] G. Y. Huang, G. Pastore, B. D. Wirth, First-principles study of intrinsic point defects
862 and Xe impurities in uranium monocarbide, Journal of Applied Physics 128 (2020).
863 [doi:10.1063/5.0021951](https://doi.org/10.1063/5.0021951).
- 864 [70] J. Liu, C. Gasparrini, J. T. White, K. Johnson, D. A. Lopes, V. K. Peterson, A. Studer,
865 G. J. Griffiths, G. R. Lumpkin, M. R. Wenman, P. A. Burr, E. S. Sooby, E. G. Obbard,
866 Thermal expansion and steam oxidation of uranium mononitride analysed via in situ
867 neutron diffraction, Journal of Nuclear Materials 575 (2023). [doi:10.1016/j.jnucmat.2022.154215](https://doi.org/10.1016/j.jnucmat.2022.154215).
- 869 [71] C. O. T. Galvin, N. Kuganathan, N. J. Barron, R. W. Grimes, Predicted thermo-
870 physical properties of UN, PuN, and (U,Pu)N, Journal of Applied Physics 135 (16)
871 (2024) 165101. [arXiv:
https://pubs.aip.org/aip/jap/article-pdf/doi/10.1063/5.0177315.pdf](https://pubs.aip.org/aip/jap/article-pdf/doi/10.1063/5.0177315/19894692/165101\1\5.0177315.pdf), [doi:10.1063/5.0177315](https://doi.org/10.1063/5.0177315).
873 URL <https://doi.org/10.1063/5.0177315>
- 874 [72] J. B. Wachtman, W. E. Tefft, D. G. Lam, C. S. Apstein, Exponential temperature
875 dependence of Young's modulus for several oxides, Physical Review 122 (1961) 1754–
876 1759.
- 877 [73] M. D. Salleh, J. E. Macdonald, G. A. Saunders, P. de V Du Plessis, Hydrostatic pres-
878 sure dependences of elastic constants and vibrational anharmonicity of uranium nitride,
879 Journal of Materials Science 21 (1986) 2577–2580.
- 880 [74] S. L. Hayes, J. K. Thomas, K. L. Peddicord, Material property correlations for uranium
881 mononitride II. mechanical properties, Journal of Nuclear Materials 171 (1990) 271–288.
- 882 [75] A. Padel, C. de Novion, Constantes elastiques des carbures, nitrures et oxydes d'uranium
883 et de plutonium, Journal of Nuclear Materials 33 (1969) 40–51.
- 884 [76] D. Frazer, B. Maiorov, U. Carvajal-Nuñez, J. Evans, E. Kardoulaki, J. Dunwoody, T. A.
885 Saleh, J. T. White, High temperature mechanical properties of fluorite crystal structured
886 materials (CeO_2 , ThO_2 , and UO_2) and advanced accident tolerant fuels (U_3Si_2 , UN, and
887 UB_2), Journal of Nuclear Materials 554 (2021). [doi:10.1016/j.jnucmat.2021.153035](https://doi.org/10.1016/j.jnucmat.2021.153035).
- 888 [77] C. Zener, Contributions to the theory of beta-phase alloys, Physical Review 71 (1947).
889 [doi:10.1103/PhysRev.71.846](https://doi.org/10.1103/PhysRev.71.846).
- 890 [78] J. Adachi, K. Kurosaki, M. Uno, S. Yamanaka, M. Takano, M. Akabori, K. Minato, Me-
891 chanical properties at sub-microscale and macroscale of polycrystalline uranium mononi-
892 tride, Journal of Nuclear Materials 384 (2009). [doi:10.1016/j.jnucmat.2008.09.019](https://doi.org/10.1016/j.jnucmat.2008.09.019).
- 893 [79] H. L. Whaley, W. Fulkerson, R. A. Potter, Elastic moduli and Debye temperature of
894 polycrystalline uranium nitride by ultrasonic velocity measurements, Journal of Nuclear
895 Materials 31 (1969). [doi:10.1016/0022-3115\(69\)90234-7](https://doi.org/10.1016/0022-3115(69)90234-7).
- 896 [80] E. F. Westrum, C. M. Barber, Uranium mononitride: Heat capacity and thermodynamic
897 properties from 5 to 350 K, The Journal of Chemical Physics 45 (1966) 635–639.

- 898 [81] V. G. Baranov, Y. N. Devyatko, A. V. Tenishev, A. V. Khlunov, O. V. Khomyakov, A
899 physical model for evaluating uranium nitride specific heat, Journal of Nuclear Materials
900 434 (2013). [doi:10.1016/j.jnucmat.2012.10.047](https://doi.org/10.1016/j.jnucmat.2012.10.047).
- 901 [82] D. P. Sellan, E. S. Landry, J. E. Turney, A. J. McGaughey, C. H. Amon, Size effects in
902 molecular dynamics thermal conductivity predictions, Physical Review B - Condensed
903 Matter and Materials Physics 81 (2010). [doi:10.1103/PhysRevB.81.214305](https://doi.org/10.1103/PhysRevB.81.214305).
- 904 [83] J. A. Jackman, T. M. Holden, J. I. Buyers, P. de V. DuPlessis, O. Vogt, J. Genossar,
905 Systematic study of the lattice dynamics of the uranium rocksalt-structure compounds,
906 Physical Review B 33 (1986) 7144–7153.
- 907 [84] A. A. Aczel, G. E. Granroth, G. J. MacDougall, W. J. Buyers, D. L. Abernathy, G. D.
908 Samolyuk, G. M. Stocks, S. E. Nagler, Quantum oscillations of nitrogen atoms in ura-
909 nium nitride, Nature Communications 3 (2012). [doi:10.1038/ncomms2117](https://doi.org/10.1038/ncomms2117).
- 910 [85] X. W. Zhou, S. Aubry, R. E. Jones, A. Greenstein, P. K. Schelling, Towards more
911 accurate molecular dynamics calculation of thermal conductivity: Case study of {GaN}
912 bulk crystals, Physical Review B - Condensed Matter and Materials Physics 79 (2009).
913 [doi:10.1103/PhysRevB.79.115201](https://doi.org/10.1103/PhysRevB.79.115201).
- 914 [86] N. W. Ashcroft, N. D. Mermin, Solid State Physics, 1st Edition, Cengage Learning,
915 1976.
- 916 [87] X. Li, P. F. Liu, E. Zhao, Z. Zhang, T. Guidi, M. D. Le, M. Avdeev, K. Ikeda, T. Otomo,
917 M. Kofu, K. Nakajima, J. Chen, L. He, Y. Ren, X. L. Wang, B. T. Wang, Z. Ren,
918 H. Zhao, F. Wang, Ultralow thermal conductivity from transverse acoustic phonon
919 suppression in distorted crystalline α -MgAgSb, Nature Communications 11 (2020). [doi:
920 10.1038/s41467-020-14772-5](https://doi.org/10.1038/s41467-020-14772-5).
- 921 [88] Z. Tian, K. Esfarjani, J. Shiomi, A. S. Henry, G. Chen, On the importance of optical
922 phonons to thermal conductivity in nanostructures, Applied Physics Letters 99 (2011).
923 [doi:10.1063/1.3615709](https://doi.org/10.1063/1.3615709).
- 924 [89] S. L. Hayes, J. K. Thomas, K. L. Peddicord, Material property correlations for uranium
925 mononitride III. transport properties, Journal of Nuclear Materials 171 (1990) 289–299.
- 926 [90] F. A. Kröger, H. J. Vink, Relations between the concentrations of imperfections in
927 crystalline solids, Solid State Physics - Advances in Research and Applications 3 (1956).
928 [doi:10.1016/S0081-1947\(08\)60135-6](https://doi.org/10.1016/S0081-1947(08)60135-6).
- 929 [91] J. T. White, A. T. Nelson, J. T. Dunwoody, D. D. Byler, D. J. Safarik, K. J. McClellan,
930 Thermophysical properties of U_3Si_2 to 1773 K, Journal of Nuclear Materials 464 (2015).
931 [doi:10.1016/j.jnucmat.2015.04.031](https://doi.org/10.1016/j.jnucmat.2015.04.031).
- 932 [92] Y. Lu, B. T. Wang, R. W. Li, H. L. Shi, P. Zhang, Structural, electronic, mechanical, and
933 thermodynamic properties of UN_2 : Systematic density functional calculations, Journal
934 of Nuclear Materials 410 (2011) 46–51. [doi:10.1016/j.jnucmat.2010.12.308](https://doi.org/10.1016/j.jnucmat.2010.12.308).

- 935 [93] J. S. Olsen, L. Gerward, U. Benedict, New high-pressure phase of uranium nitride stud-
936 ied by X-ray diffraction and synchrotron radiation., Journal of Applied Crystallography
937 18 (1985). [doi:10.1107/S0021889885009736](https://doi.org/10.1107/S0021889885009736).
- 938 [94] P. Modak, A. K. Verma, First-principles investigation of electronic, vibrational, elastic,
939 and structural properties of ThN and UN up to 100 GPa, Physical Review B - Condensed
940 Matter and Materials Physics 84 (2011). [doi:10.1103/PhysRevB.84.024108](https://doi.org/10.1103/PhysRevB.84.024108).
- 941 [95] J. Rösler, H. Harders, M. Bäker, Mechanical Behaviour of Engineering Materials,
942 Springer, 2007.
- 943 [96] H. E. Rosinger, D. O. Northwood, The elastic properties of zirconium alloy fuel cladding
944 and pressure tubing materials, Journal of Nuclear Materials 79 (1979). [doi:10.1016/0022-3115\(79\)90444-6](https://doi.org/10.1016/0022-3115(79)90444-6).
- 945 [97] C. Kittel, Introduction to Solid State Physics, 8th Edition, John Wiley & Sons, Inc,
946 2005.